The dynamics of diluted bitumen derived oil-mineral aggregates, Part I.

Casey O'Laughlin, Brent A. Law, Vanessa S. Zions, Thomas L. King, Brian Robinson, Yongsheng Wu

Science Branch
Fisheries and Oceans Canada
P.O. Box 1006
1 Challenger Drive
Dartmouth NS Canada B2Y 4A2

2016

Canadian Technical Report of
Fisheries and Aquatic Sciences No. 3157

Fisheries and Oceans Canada | Pêches et Océans Canada

Canada

Canadian Manuscript Report of Fisheries and Aquatic Sciences

Manuscript reports contain scientific and technical information that contributes to existing knowledge but which deals with national or regional problems. Distribution is restricted to institutions or individuals located in particular regions of Canada. However, no restriction is placed on subject matter, and the series reflects the broad interests and policies of Fisheries and Oceans Canada, namely, fisheries and aquatic sciences.

Manuscript reports may be cited as full publications. The correct citation appears above the abstract of each report. Each report is abstracted in the data base *Aquatic Sciences and Fisheries Abstracts*.

Manuscript reports are produced regionally but are numbered nationally. Requests for individual reports will be filled by the issuing establishment listed on the front cover and title page.

Numbers 1-900 in this series were issued as Manuscript Reports (Biological Series) of the Biological Board of Canada, and subsequent to 1937 when the name of the Board was changed by Act of Parliament, as Manuscript Reports (Biological Series) of the Fisheries Research Board of Canada. Numbers 1426 - 1550 were issued as Department of Fisheries and Environment, Fisheries and Marine Service Manuscript Reports. The current series name was changed with report number 1551.

Canadian Technical Report of
Fisheries and Aquatic Sciences No.

2016

The dynamics of diluted bitumen derived oil-mineral aggregates, Part I.

by

Casey M. O'Laughlin[1], Brent A. Law[1], Vanessa S. Zions[1], Thomas L. King[2], Brian Robinson[2], Yongsheng Wu[1]

[1]Coastal Ecosystem Science Division
Science Branch
Fisheries and Oceans Canada
P.O. Box 1006
1 Challenger Drive
Dartmouth NS Canada B2Y 4A2

[2]Center for Offshore Oil, Gas and Energy Research
Fisheries and Oceans Canada
P.O. Box 1006
1 Challenger Drive
Dartmouth NS Canada B2Y 4A2

Cat. No. Fs 97-6/3157E ISBN 978-0-660-04596-2 ISSN 0706-6457 (print)
Cat. No. Fs 97-6/3157E-PDF ISBN 978-0-660-04597-9 ISSN 1488-5379 (online)

Correct citation for this publication:

O'Laughlin *et al.*, 2016. The dynamics of diluted bitumen derived oil-mineral aggregates, Part I. Can. Tech. Rep. Fish. Aquat. Sci. 3157: viii + 44p.

CONTENTS

LIST OF TABLES

LIST OF FIGURES

ABSTRACT

The export of Canadian diluted bitumen to international markets via the Pacific Ocean requires an ocean-based segment in the proposed transport route. This introduces the risk of oil being released into the marine environment, and necessitates an oceanographic perspective on potential spills. Parameters such as the size, settling velocity and bulk density of naturally formed oil-mineral aggregates (OMA) are primary constituents in predictive models for evaluating the potential fate of oil spilled in the aquatic environment. This report presents results from one series of low sediment concentration (15 mg L^{-1}), colder water (< 10°C) wave tank experiments, designed to measure variability in size, settling velocity and density of naturally formed OMA in response to bitumen type, sediment concentration and the use of chemical dispersant. High-resolution imagery of settling particles collected with digital floc cameras in the wave tank were analyzed for particle size, density and settling velocity. OMA were not readily identifiable in imagery collected from the wave tank, likely due to the limited time scale for formation during experiments. Possible effects of chemical dispersant on natural sediment flocculation, the size of suspended oil droplets and the clearance rate of suspended particles are discussed. Results of lab experiments designed to measure OMA particle size, settling velocity and total petroleum hydrocarbon (TPH) sedimentation, under different sediment concentration scenarios (10, 50 and 100 mg L^{-1}), suggest that average particle size and settling velocity increase with sediment concentration: 99.34 μm and 0.35 mm·s^{-1}, at 50 mg L^{-1}, compared with 65.71 μm and 0.15 mm·s^{-1}, at 10 mg L^{-1}. TPH sedimentation results show that increasing the sediment load from 50 to 100 mg L^{-1} can produce a decrease in TPH sedimentation.

RÉSUMÉ

L'exportation de bitume dilué canadien vers des marchés internationaux par l'entremise de l'océan Pacifique nécessite un segment océanique dans l'itinéraire de transport proposé. Le pétrole risque ainsi d'être déversé dans le milieu marin, et l'exportation nécessite donc une perspective océanographique sur les déversements potentiels. Des paramètres tels que la taille, la vitesse de sédimentation et la densité apparente des agrégats d'hydrocarbures et de minéraux naturellement formés représentent des constituants primaires des modèles de prévision pour l'évaluation du devenir potentiel des déversements de pétrole dans l'environnement aquatique. Ce rapport présente les résultats d'une série d'expériences effectuées dans des réservoirs d'eau plus froide (< 10 °C) à faible concentration de sédiments (15 mg L^{-1}). Ces expériences ont été conçues pour mesurer la variabilité de la taille, de la vitesse de sédimentation et de la densité des agrégats d'hydrocarbures et de minéraux en réponse au type de bitume, à la concentration des sédiments et à l'utilisation d'agents dispersants chimiques. Des images de haute résolution de la sédimentation de particules, qui ont été recueillies à l'aide de caméras numériques de silhouettage du floc dans le réservoir d'eau, ont été analysées pour déterminer la taille, la densité et la vitesse de sédimentation des particules. Les agrégats d'hydrocarbures et de minéraux n'étaient pas en mesure d'être détectés dans les images recueillies du réservoir d'eau, principalement en raison des délais de formation limités durant les expériences. Les effets possibles des agents dispersants chimiques sur la floculation des sédiments naturels, sur la taille des gouttelettes de pétrole en suspension et sur le taux d'élimination des particules en suspension sont abordés. Les résultats des expériences de laboratoire conçues pour mesurer la taille des particules d'agrégats d'hydrocarbures et de minéraux, la vitesse de sédimentation et le total de sédimentation des hydrocarbures pétroliers dans différents scénarios de concentration de sédiments (10, 50 et 100 mg L^{-1}) suggèrent qu'une vitesse de sédimentation et une taille de particules moyennes augmentent avec la concentration de sédiments. Les résultats propres à la sédimentation totale des hydrocarbures pétroliers démontrent que l'augmentation de la charge de sédiments de 50 à 100 mg L^{-1} peut entraîner une diminution de la sédimentation totale des hydrocarbures pétroliers.

PREFACE

The following technical report, '*The dynamics of diluted bitumen derived oil-mineral aggregates, Part I*' is the initial assemblage of data generated by a series of experiments in the wave tank facility operated by the Centre for Offshore Oil, Gas and Energy Research (COOGER) at Bedford Institute of Oceanography. The reported series of experiments ran from April to October 2014.

Experiments summarized and discussed herein comprise the low sediment concentration (15 mg L^{-1}), cold water (<10 °C) portion of wave tank testing. Additional testing will be reported on in the near future, to describe experiments conducted with warmer water (>10 °C) and higher sediment concentration (50 mg L^{-1}).

This report is a product of the Particle Dynamics Lab with support from COOGER, at the Bedford Institute of Oceanography, in Dartmouth, Nova Scotia.

1.0 INTRODUCTION

1.1 INITIATIVE

The World Class Tanker Safety (WCTS) program is a Government of Canada initiative aimed at improving the overall operating environment of the oil transport industry in Canada. This program coincides with large-scale pipeline projects proposed to move Alberta crude oil products to market, such as the Enbridge Northern Gateway and Keystone XL projects. The Northern Gateway proposal involves transporting diluted bitumen westward via pipeline from northeastern Alberta, and then by sea out of Kitimat, British Columbia via Douglas Channel. The ocean-based portion of this transport route introduces the risk of oil products being released into the marine environment, and necessitates an oceanographic perspective on the response to potential spills.

1.2 BACKGROUND

The settling and subsequent deposition of fine-grained suspended particles in the marine environment is influenced by the flocculation process, or the grouping of discrete particles into loosely-packed aggregates known as flocs (Kranck, 1973, McCave, 1984, Kranck, 1985, Kranck and Milligan 1992; Milligan *et al.*, 2007). A flocculated suspension is the result of a balance between forces that encourage floc growth through inter-particle encounters, such as suspended sediment concentration and particle adhesion efficiency, and the turbulent shear forces that pull flocs apart (Milligan and Law, 2005; Manning and Dyer, 2002). Due to their increased size, flocs settle faster than their constituent particles (Sternberg *et al.*, 1999; Curran *et al.*, 2007). As flocculation rate increases, the flux of fine-grained material to the seabed increases as well. The majority of fine-grained sediments present on the seabed are deposited within flocs (Kranck, 1980; Curran *et al.*, 2002).

Parameters that describe fine-sediment dynamics such as flocculation are critical elements of complex sediment transport-hydrodynamic models, designed for functionality in the near-shore and coastal zones. Similarly, the evaluation of the potential fate of oil spilled in the aquatic environment is primarily completed through predictive modelling, which incorporates parameters describing the dynamics of oil-mineral aggregates (OMA). Similar to flocculation, the formation of OMA is primarily influenced by the concentration of suspended particulate matter (SPM) and the level of mixing energy (Khelifa *et al.*, 2005; Li *et al.*, 2008; Sun *et al.*, 2013). As wave action, tidal mixing or chemical dispersants break-up oil slicks on the water surface, oil droplets become coated with micron-scale fine sediment available in the water column. This coating stabilizes the droplets and reduces their stickiness, which prevents droplet recoalescence and decreases adherence to surfaces in the coastal zone (Page *et al.*, 2000; Lee *et al.*, 2003). Density increases as oil droplets are covered in sediment, and eventually this leads them to sink into the water column, where rates of mineralization by bacterial and planktonic species are enhanced and the oil biodegrades (Venosa and Holder, 2007; Lindstrom and Braddock, 2002).

Most OMA formation is linked to the presence of fine particles and occurs at or above a 50 mg L^{-1} sediment concentration (Khelifa *et al.*, 2008b); although concentrations as low as 10 mg L^{-1} have been shown to produce OMA in laboratory experiments (Ajijolaiya *et al.* 2006). A critical sediment concentration for maximized OMA formation has been discussed by Ajijolaiya *et al.* (2006), where all suspended oil droplets are covered by a monolayer of fine grains. The critical concentration was found to increase linearly with particle size, ranging from 200 mg L^{-1} for 1 µm particles to 490 mg L^{-1} for 16 µm particles. With increasing sediment concentration, the percentage of oil trapped in OMAs is amplified to maxima that vary with oil type (Khelifa *et al.*, 2007). Other factors relevant to OMA formation include oil viscosity (Khelifa *et al.*, 2002; 2007), the effects of salinity and sediment type (Khelifa *et al.*, 2005) and other sedimentary properties (Zhang *et al.*, 2010). One notable effect is the hydrophobicity of minerals, which can promote bonds between sediment and oil particles and encourage OMA formation (Wang *et al.*, 2013; Wang *et al.*, 2011). However, when applied, chemical dispersants (e.g. Corexit 9500) are the dominate influence on the formation and behaviour of OMA (Zhang *et al.*, 2010). Dispersants chemically break down oil slicks by reducing oil-water interfacial tension and facilitating a decrease in oil and OMA droplet size distribution. This accelerates and increases the overall transfer of oil from the surface downward into the water column, compared with instances of natural, physical dispersion (Li *et al.*, 2007; 2008). The presence of chemical dispersant dominates oil-sediment interactions and overcomes natural oil-sediment sinking dynamics, promoting suspensions of small dispersed oil particles (Lee *et al.* 2008), although many oil particles can re-coalesce and float back to the water surface (Zhang *et al.*, 2010).

The presence and behaviour of OMA has become an increasingly relevant topic, including research into the time scale and kinetics of OMA formation (Hill *et al.*, 2002; Sun *et al.*, 2013; Sun *et al.*, 2014). Studies on the transport and fate of OMA are limited, as are the parameters required to initiate transport models capable of prediction (Niu *et al.*, 2011; Gong *et al.*, 2014). In addition, diluted bitumen, known as dilbit, has not been extensively considered in previous efforts to determine the behaviour and fate of oil particles in the marine environment, with the exception of recently emerging research (e.g. King *et al.*, 2014; Government of Canada, 2013; Lee *et al.*, 2012). Dilbit is a combination of heavy bitumen oil and lighter diluent, which is added to bitumen to decrease its viscosity and density for transport. Topics including the formation of OMA from diluted bitumen, the behaviour of these aggregate particles and the influence of chemical dispersant on the formation and behaviour of dilbit-derived OMA have not been widely considered. A recent report (Government of Canada, 2013) suggests that dilbit sinks with sufficient mixing in the presence of medium to fined-grained sediment. The same report identified knowledge gaps regarding the exact conditions which allow dilbit to sink in the marine environment. It has been shown that dilbit is capable of forming OMA and sinking in freshwater conditions (Lee *et al.*, 2012), and that the chemical composition of various dilbit products has an influence on its fate and behaviour in the marine environment (King *et al.*, 2014). It is highly desirable to expand this knowledge toward a thorough understanding of the fate and behaviour of dilbit released into the marine environment.

The primary goal of the research described here is to measure variability in particle size and settling velocity of OMA, in response to changes in: (1) suspended sediment concentration, (2) the presence of chemical dispersants, (3) the type of oil, and (4) the level of mixing energy. This is addressed through a combination of large-scale wave tank experiments and smaller-scale laboratory experiments. Ultimately, transport parameters derived from this research will be applied in predictive modelling studies of the transport and fate of OMA in the environment. These parameters include the particle size distribution and settling velocity of OMA, and the percentage of settled oil (Niu *et al.*, 2011).

2.0 METHODOLOGY

2.1 GENERAL APPROACH

This research effort is comprised of a series of wave tank (Table 1) and complementary laboratory experiments to investigate OMA formation under different conditions. Wave tank experiments are designed to simulate in situ conditions for OMA formation, and allow measurements of particle size and settling velocity and estimates of particle density under changing experimental conditions (Table 2). For this report, eight colder water (< 10°C) experiments are considered in detail, which are grouped into dispersed and non-dispersed categories (Table 3). In addition, a series of lab experiments have been completed to (1) investigate the size and settling velocity of OMA, and (2) to determine the ratio of oil to sediment present in OMA.

2.2 DATA COLLECTION

2.2.1 Wave tank experiments

Experiments in the wave tank facility operated by the Centre for Offshore Oil, Gas and Energy Research (COOGER) at the Bedford Institute of Oceanography began in April 2014. Twenty experiments were completed in total, using dispersed and non-dispersed samples of weathered Access Western Blend (AWB) (12 experiments) and Cold Lake Blend (CLB) (6 experiments) diluted bitumen. Two additional experiments were completed using only sediment, with no oil or dispersant. The sediment component used in all experiments was fine-grained material sourced from 2 locations in Douglas Channel. A range of 800-1500 grams of material was added to the tank, dependant on the sediment moisture content, to achieve a sediment concentration of 15 mg L^{-1}. When dispersant was applied, Corexit 9500 was used, at a dispersant-to-oil ratio (DOR) of 1:20. Wave tank experiments were spread over summer and winter seasons to account for seasonal variability (e.g. temperature) in OMA formation.

Sediment used in wave tank experiments was sourced from two locations in Douglas Channel, along the proposed transport route (Figure 1). Samples were collected in summer 2013 (DC-09) and winter 2014 (DC-26) via an Ekman grab from CGGS Tully (Table 2). Station numbers indicate the distance from Kitimat, in nautical miles. Sediment from two locations was used in wave tank testing to ensure the full range of sediment type and grain size that occurs along the channel is represented. Sediment was first analyzed for disaggregated inorganic grain size (DIGS) using a Coulter Multisizer III electro-resistance particle counter, following methods described by Milligan and Kranck (1991), Kranck and Milligan (1979) and Law *et al.* (2012). The majority of Douglas Channel bottom material is mud, with a sand component of less than 1%, covering a size range of 1-73 μm. Modal diameters and d50 values are 10.5 μm and 8.0 μm respectively for DC-09, and 2.6 μm and 5.0 μm for DC-26. Along-channel variations in particle size suggest that bottom sediments from the lower segment of Douglas Channel (e.g. DC-26) are slightly finer than material found in the upper portion of the channel (e.g. DC-09).

The wave tank facility is comprised of a 40 meter long tank, measuring 2 m deep and 60 cm wide with an average water level in the tank of 1.5 meters (Figure 2). The computer-controlled wave-generating paddle is located 1 meter from the end of the tank, and can produce both regular non-breaking and breaking waves of designated length, height, and frequency. To minimize wave reflection, wave energy is absorbed at the back of the tank by a series of porous screens. During wave production, each wave train lasts approximately 15 seconds and includes a set of 3 breaking waves, followed by 25 seconds of quiescence. Maximum peak-to-trough wave amplitude is 45 cm. This system is designed to simulate the propagation and breaking of deep-water waves, based on linear wave theory (Li *et al.*, 2007; 2008). Each wave tank experiment was composed of four 1-hour phases: (1) mixing 'A' (sediment only), (2) mixing 'B' (sediment, oil), (3) settling and (4) flushing. Bedford Basin seawater was pumped through three sock filters (25 μm, 5 μm and 5 μm) and into the wave tank just prior to experiments. Sediment was added and waves generated for a total of 2 hours during the mixing phases. After 1 hour of mixing, oil (and dispersant, if required) was added to the tank, followed by another hour of mixing. Waves were turned off during the settling phase, and back on for the flushing phase to end each experiment.

For the duration of wave tank experiments, high-resolution images (3296 x 2472 pixels; 93.8 pixels/mm) of suspended and settling particles were collected with two machine-vision floc cameras (MFVC) (model Prosilica GX3300 from Allied Vision, 8.0 megapixel), with measurement ranges of 45 μm to 1mm. One camera was positioned approximately 10 meters from the wave generating paddle, with the sampling volume at 35 cm below the surface, and collected one image every 30 seconds. The camera was co-located with a Laser in-situ Scattering and Transmissometry (LISST) 100-X particle size analyzer (type C), which sampled every 3 seconds over a measurement range of 2.5 to 500 μm. Together, these datasets cover the full range of anticipated particle sizes. The velocity of settling particles was measured with a second, further-specialized floc camera, known as the size versus settling MVFC (SVS-MVFC). This instrument is equipped with a rectangular settling column (50×10×5 cm) with baffled top above the field of view. During each wave tank experiment, this camera acquired a continuous 30-second stream of images at 5-minute intervals (at 11 frames per second). During wave tank experiments, the SVS-MVFC was placed on the bottom of the tank, 17.5 meters from the paddle (~2/3 of the tank length). The baffled top through which particles fall was positioned at 80 cm depth, with the enclosed sampling volume at 130 cm depth.

Image analysis to derive particle size and size versus settling relationships was completed in MATLAB. Raw image files were converted to greyscale bitmaps using ImageJ. The threshold grayscale value, used to differentiate particle edges from the image background, was defined using Otsu's method for SVS-MVFC images, and triangle method for MFVC images (Mikkelsen *et al.*, 2007; Fox *et al.*, 2004). Where necessary, images were cropped to exclude obstructions, such as smudges on the camera window. Grain size statistics (particle area, shape descriptors, diameter, and perimeter) were calculated, and particle sizes derived from MFVC images were binned to compliment LISST data. Particle size data generated from the MFVC (45 μm – 1 mm) were manually merged with that of the LISST (2.5 – 500 μm) to produce continuous grain size spectra (2.5 μm – 1 mm). Merging began at the 63 μm bin, where the resultant value is derived from 50% LISST data and 50% MFVC data. From there, the ratio of value contributions from each dataset was changed in 10% increments per bin (e.g. 60-40, 70-30, etc), in favor of the dataset with the appropriate size range. The resulting merge of camera and LISST datasets occurs over 9 size bins. Merged particle size distributions are shown with the log of particle diameter (μm) plotted against the log of volume concentration (ppm). Size-settling velocity relationships and effective densities were estimated from images collected with the SVS-MVFC. Four frames, separated by one second in time, were overlain to produce a composite image, which was used to derive continuous tracks for individual particles across the sensing zone.

Stagnant particles were deleted during the MATLAB routine. Particles from each frame appear numbered and color-coded in composite images, allowing individual particles to be manually tracked (Mikkelsen *et al.*, 2004). Settling velocity is calculated using the distance travelled and the time between images in MATLAB. Finally, the bulk density of settling aggregates was estimated using an inverted Stoke's law method (Fox *et al.*, 2004; Curran *et al.*, 2007).

Water temperature (°C) and salinity (ppt) were measured with a handheld YSI system (model 30M). Water samples were drawn from the tank to monitor the concentration and distribution of suspended materials. Samples were drawn from 3 locations in the tank (positions A, B and D), at up to 3 depths, every 15-20 minutes; this sampling scheme results in approximately 70 samples per experiment. Samples were drawn at two depths at position A (5 and 145 cm), one depth at position B (35 cm), and up to three depths at position D (5, 75 and 145) (Figure 2). Sampling intensity was increased at position D during settling phases, while position A was not sampled during settling phases. Using standard gravimetric methods, water samples were vacuum filtered onto pre-weighed Millipore 8.0 μm cellulose filters. These were dried (24 hours at 60°C), weighed, compared to pre-weights and divided by the volume of sample water filtered to determine the concentration (Law *et al.*, 2008). Water samples were also filtered to characterize the natural background concentration in the experiment water from the Bedford Basin, and were processed for organic content (Table 3). These filters (Whatman 25 mm glass fiber) are pre-washed, combusted at 550°C for 12 hours, and weighed prior to use.

2.2.2 Lab experiments

To determine the settling velocity of formed OMAs, Douglas Channel (DC-09) sediment was combined with diluted bitumen (AWB), Corexit 9500 dispersant (DOR 1:20) and 0.2 μm filtered Bedford Basin seawater (density of 1028 kg m^{-3}) in the lab, following the methods of Li *et al.* (2007, 2008). Mixtures were agitated on a MaxQ 2000 orbital shaker table (Fisher Scientific, USA) for 1-2 hours and left to settle overnight (~20 hours). The presence of OMA in each sample was confirmed via microscope. Settled materials were extracted with a wide-mouth pipette and gently added to the top of the settling column on the SVS-MVFC. The camera was placed in a fiberglass tank filled with Bedford Basin seawater (filtered at 15 μm), and recorded one minutes worth of images (at 11 frames per second) at 5 minute intervals over the 2 hour experiment. This experiment was completed using two different concentrations of Douglas Channel sediment (10 and 50 mg L^{-1}), with similar water temperature and salinity conditions (~6.0°C and 32.0 ppt).

Additional lab experiments were conducted to measure the amount of oil associated with sinking sediment particles, using a modified version of the Baffle Flask

Test (Venosa *et* al., 2002). Experiments considered three unique sediment concentration scenarios (0, 10 and 50 mg L^{-1}), and their interaction with two concentrations of oil-dispersant solution. Sediment was combined with filtered Bedford Basin seawater to produce 1 L of stock solution, for the zero-sediment control and each of the three sediment concentrations (10, 50 and 100 mg L^{-1}). An oil and dispersant stock, containing AWB dilbit and Corexit 9500 (DOR 1:20), was pre-mixed and added to 100 ml of seawater/sediment stock using a positive displacement Drummond Digital Microdispenser (Drummond Scientific Co, USA). Either 5 or 20 µL of the oil/dispersant premix was carefully added to each flask to achieve an oil concentration of 50 or 200 ppm. Flasks were then mixed for 2 hours at 200 rpm on the shaker table. After mixing, samples were transferred to a graduated cylinder and left to settle for 24 hours. The upper 90 ml of the water phase (including any oil that surfaced) was then removed with by siphon. The remaining 10 ml was gently agitated and vacuum-filtered through Whatman GF/C glass fibre filters to collect settled materials. After air drying for 24 hours, filters were processed to determine the total amount of oil that had sunk to the bottom with the sediments. Oil was extracted from the filters using a Soxhlet extractor and dichloromethane (DCM) over an 18-hour period. Following extraction, DCM was concentrated to a final volume of 1 mL using a Zymark evaporator, and transferred into an autosampler vial and stored at -20°C for analysis of Total Petroleum Hydrocarbons (TPH). A detailed description of the protocol used for measuring TPH can be found in King *et al.* (2015).

3.0 RESULTS

3.1 WAVE TANK EXPERIMENTS

Prior to the addition of sediment, the background concentration in wave tank experiment water ranged from ~1.0 - 2.5 mg L^{-1}, with 50 – 80% of that material being organic (Table 3). The sediment concentration derived from water samples drawn from the wave tank is shown in Figures 3 to 5. In general, initial concentration of ~20 mg L^{-1} gradually decreased to ~10 mg L^{-1} by experiment end. Samples from position A showed that material stabilized at 10-20 mg L^{-1} at 5 and 145 cm depths within 20 minutes of adding sediment to the tank (Figure 3). Similar concentration levels were measured in samples collected at position ‘B’ (Figure 4). At the other end of the tank, at position ‘D’, SPM concentration was stable at 10-20 mg L^{-1} after approximately 40 minutes of mixing (Figure 5). During wave tank experiment 12 (WTE-12), SPM concentration reached levels that were marginally higher than other experiments, at each sampling location. This typically began early in the experiment, during the first mixing phase. However, during the settling phase at position B, an appreciable increase to 30 mg L^{-1} occurred. Aside from initial spikes to high concentration immediately following the addition of sediment, this sample constitutes the maximum SPM concentration measured during all experiments, suggesting that sediment was generally well distributed in the tank.

Merged particle size distributions obtained from MVFC images and LISST data show maximum particle sizes of suspended material in the wave tank ranging from 460-750 μm. Grain size curves derived from these data are predominantly bimodal (Figures 6 to 13). For analysis, merged camera and LISST data from each wave tank experiment were separated into the three, hour-long phases of interest: mixing A (sediment only), mixing B (sediment, oil and dispersant), and settling (waves off). Images collected at 5- and 15-minute increments (t = 0, 5, 15, 30, 45 and 60) throughout each phase were considered for analysis. Figures 6-13 show merged grain size curves and the associated MVFC images, collected (1) just prior to the addition of oil, (2) when oil was added, and (3) immediately after. The mud fraction (< 63 μm) typically increased from 10-20% to 40-50% in the 10-15 min period after sediment was added, as smaller particles gradually reached instrument sensing zones at 35 cm depth. The period following the addition of oil (and dispersant where applicable) shows an increased volume of particles > 100 μm in the 5-10 minutes after oil and dispersant are applied, as oil particles are driven into the water column by waves. Concentration rapidly decreases after 5-10 minutes as oil distributes down the tank. This is followed by a more gradual decrease over a 20-60 minute period. Where dispersant is used, this phase is accompanied by a rapid decrease in the < 63 μm fraction (from 40-50% down to 10-20%). Similar decreases are either absent or less drastic where dispersant was not used, and in some cases are contrasted by an increase in the < 63 μm fraction, potentially representing larger oil droplets in suspension. By the end of the mixing ‘B’ phase, the typical size distribution closely reflected that prior to the addition of oil and/or dispersant. Over the hour-long settling phases, depletion of smaller grain sizes (< 45 μm) was typical, as sediment gradually flocculated and smaller particles were incorporated into larger flocs. This theoretically translates into a complementary increase in particle size, and growth at the coarse end of grain size curves was observed during 5 of the 8 experiments reported here. These generally corresponded with experiments where dispersant was not used. Depletion of smaller grain sizes (< 45 μm) was most pronounced during 3 experiments in particular, although these instances were not consistently accompanied by subsequent particle growth.

The size of dispersed oil droplets in suspension was determined using simple subtraction of grain size data generated by the MVFC (Figure 14), from images captured pre- and post-oil. Camera data was chosen specifically for this exercise due to the notable change in volume at 100-400 μm. Size distributions representing dispersed oil conditions typically show bimodal peaks around 200 μm, and a maximum oil droplet size of 400-700 μm. This is larger than under non-dispersed conditions, which showed maximum particle sizes of 260-400 μm and have no clearly discernable mode. This suggests that the presence of dispersed oil droplets in the water column constitutes the noted increase in particle size. During non-dispersed conditions, only a limited number of oil droplets penetrate the water column, and thus the size distribution of suspended material in these instances is dominated by sediment. This explains why oil droplet size is notably smaller during non-dispersed experiments, and suggests that non-dispersed dilbit resists sinking, at least on the time scale tested.

Size versus settling relationships from wave tank experiments show mean, per-experiment particle sizes ranging from 70 to 105 μm, and average settling velocities on the order of 0.2 $mm \cdot s^{-1}$ (Table 4). Figures 15 - 21 show that overall, particle size (36 - 450 μm) and settling velocity (0.03 - 17.7 $mm \cdot s^{-1}$) of individual particles covered wide ranges. Mean values of effective particle density ranged from 50.6 to 225.5 kg m^3. The largest mean particle size (105 μm) was found under non-dispersed conditions during WTE-12; particles from this experiment also showed the lowest effective density.

3.2 LAB EXPERIMENTS

Laboratory settling experiments showed variability in size-settling relationships for 10 and 50 ppm concentrations of Douglas Channel sediment (Figure 22). At 50 ppm, average particle size and settling velocity (99.34 μm and 0.35 $mm \cdot s^{-1}$) were notably higher than at 10 ppm (65.71 μm and 0.15 $mm \cdot s^{-1}$). Particle densities were similar at 92.16 and 90.1 kg m^3 for the 50 mg L^{-1} and 10 mg L^{-1} studies.

Two oil concentrations (50, 200 ppm) and three sediment concentrations (10, 50, 100 mg L^{-1}) were considered for lab experiments designed to measure the amount of oil incorporated with settling sediment particles. Figure 23 shows the percentage of the total amount of oil that sunk to the bottom over 24 hours. In general, results show that the greatest amount of sunken oil (20-25%) was associated with higher sediment concentrations (50 & 100 mg L^{-1}), at the lower oil concentration (50 ppm). With higher sediment loads, significantly more oil was found incorporated with the sediment at the 50 ppm oil dose: total sunken oil amounts of 25.2±5.3 % with 50 mg L^{-1} sediment loading and 21.6±3.8 % at 100 mg L^{-1} sediment loading are at least five times higher than total sunken oil amounts resulting from the 200 ppm oil dose, which are low at 2.7±0.4 % with 10 mg L^{-1} sediment, 5.1±2.2 % with 50 mg L^{-1} sediment and 5.2±1.2 % with 100 mg L^{-1} sediment. In addition, the LISST particle size analyzer was used to measure the oil droplet sizes generated by baffled flask experiments. With increasing oil concentration, the size distribution of oil droplets was seen to shift toward larger sizes: at the 50 ppm oil concentration, peak droplet size was 19.9 μm, compared with 45.5 μm at the 200 ppm oil concentration.

4.0 DISCUSSION

The study discussed in this report describes dilbit dynamics during large-scale wave tank experiments, and the behaviour of this material when interacting with chemical dispersant during low suspended sediment concentration conditions. Ultimately this work aims to provide unique transport parameters for predictive modelling purposes to determine the fate of oil spilled in the marine environment. In general, dilbit-derived OMA were not readily identifiable during wave tank experiments, either in images collected with the MVFC at 35 cm depth, or with the SVS-MVFC at 130 cm depth. The absence of OMA was confirmed via microscope. The lack of OMA production is thought primarily to be a limitation of the short, 2-hour duration provided for OMA formation during wave tank experiments. An expression presented by Hill *et al.* (2002) suggests that the most common formation times for stabilized OMA range from a few minutes up to 24 hours, and that the shortest formation times occurred when oil droplets were large and sediment concentration was high. It is thought that the duration of the settling phase during wave tank experiments, at the current testable sediment concentration (15 mg L^{-1}), was simply not sufficient to facilitate the formation of OMA. Hill *et al.* (2002) also stated that stable OMA failed to form when sediment concentration was low (e.g. 20 mg L^{-1}). This suggests that the formation of OMA will be more efficient at higher concentrations (e.g. 50 mg L^{-1}), based on the results of lab experiments and previous research using other oil products (Khelifa *et al.*, 2008b; Ajijolaiya *et al.*, 2006). However, in the study of Hill *et al.* (2002), concentrations of up to 200 mg L^{-1} were required to generate OMA formation times on the scale of minutes to a few hours. Additionally, when OMA did form at lower concentrations the formation time was > 24 hours. Preliminary results from a recent 24-hour wave tank experiment, where material was allowed to settle for 22 hours from a 15 mg L^{-1} sediment concentration with oil and dispersant present, have shown that even at this extended time scale OMA did not form. However, this test has only been performed once, and will be pursued further. Overall, these findings suggest that OMA formation, on the time scale of wave tank experiments, may require a mass sediment concentration in the wave tank of > 50 mg L^{-1}.

During wave tank experiments when dispersant was applied, particle size distributions obtained from images collected with the MVFC demonstrate a rapid downward transport of dispersed oil particles into the water column (e.g. during mixing ‘B’ phase) (Figures 6-13). A comparison of dispersed and non-dispersed conditions at the onset of the mixing ‘B’ phase (t = 0) is shown in Figure 24. In general, compared with non-dispersed conditions, particles covering most of the size range are consistently more abundant at 35 cm depth within 5 minutes of applying oil when dispersant is present. The majority of these are dispersed oil droplets, which generally appear as perfect spheres, although during break-up large droplets can adopt an elongated form.

The concentration of particles sized 100-330 µm was typically found to be greater with dispersant than without, which represents a strong difference in the behaviour of dispersed versus non-dispersed dilbit. The higher concentration and particle size increase was generally limited to a 45-minute period following the addition of oil and dispersant; after that, particle size distributions were closely reflective of pre-oil conditions. During experiments with no dispersant, very low concentrations of oil droplets were detected at 35 cm depth. Some particles of appreciable size (330-390 µm) were noted, but were very limited in number and became absent within 15 minutes following the addition of oil. These results support the efficiency of chemical dispersant, but do not suggest the formation of OMAs.

In the absence of dispersant, there was no rapid change in the particle size distribution at 35 cm depth in response to the addition of oil. Rather, particle size distributions remain relatively unchanged throughout both mixing phases and into the settling phase. However, in the final stages of the settling phase, the volume of particles >100 µm began to increase. Figure 25 shows a comparison of dispersed and non-dispersed conditions at the end of the settling phase (t = 60). Dashed lines (no dispersant) clearly indicate that particle size increased notably during the final stages of the settling phase. Such an increase in particle size may be explained by OMA production; however it is more likely that the natural tendency of fine sediment to flocculate is generating larger particle sizes. Under this assumption, growth in particle sizes occurring at the end of the settling phase under non-dispersed conditions should not be attributed to OMA production. It is possible that this difference in particle size growth may be caused by dispersant interacting with sediment, coating the inorganic particles and inhibiting flocculation. Dispersants are primarily composed of surfactants and solvents, and have been shown to effectively reduce oil and OMA size distribution (Singer *et al.*, 1996; Li *et al.*, 2007; Sørensen *et al.*, 2014). Surfactants act to pull oil slicks apart by lowering their surface tension, while solvents dissolve oil droplets. Conflicting results have been presented regarding the impacts of chemical dispersants on the effectiveness of OMA formation: Page *et al.* (2000) observed that chemically dispersed oil associated less with mineral matter than physically dispersed oil, while subsequent studies by Khelifa *et al.* (2005, 2008b) and Sun *et al.* (2010) have shown that chemically dispersed oil is capable of aggregating with SPM. Fu *et al.* (2014) reported that the addition of chemical dispersant enhanced particle aggregation and the formation of marine snow, with and without the presence of oil. Under dispersed conditions in the wave tank the abrupt increase in particle size at 35 cm (following the application of oil and dispersant) represents dispersed oil droplets being driven into the water column by wave energy. By the end of the settling phase (after a period of ~45 minutes), the size distribution at this location closely reflects the distribution prior to the application of oil and dispersant. This suggests that dispersed oil particles have been either moved down into the water column, or have resurfaced. Under non-dispersed conditions, the end of the settling phase is characterized by notable particle growth. It is interesting that during experiments where dispersant was applied, the settling phase lacks a similar stage of particle growth. It is expected that particle growth through flocculation would occur in both instances, although as shown in Figure 25, this did not happen during any experiment where dispersant was applied. This may be a demonstration of the effects of dispersant on natural sediment flocculation and should be further considered.

Existing studies have described flocs settling at velocities on the order of 1.0 $mm \cdot s^{-1}$ (Hill *et al.*, 2000; Curran *et al.*, 2007). Compared to this, mean settling velocities measured in the wave tank (0.1 – 0.24 $mm \cdot s^{-1}$) are low (Table 4). Sternberg *et al.* (1999) reported a broad range of settling velocities (0.08 – 8.13 $mm \cdot s^{-1}$) for flocculated particles settling from a flood plume in the coastal zone, which compares well with the range of settling velocities measured in the wave tank. Mean per-experiment values describing size versus settling relationships indicate that both dispersed and non-dispersed scenarios show particle settling velocities on the order of 0.1 - 0.2 $mm \cdot s^{-1}$. To consider the overall rate of removal of particles from the water column, and evaluate change in the presence or absence of chemical dispersant, the effective clearance rate (w_e) was calculated. The effective, or bulk mean, clearance rate is the settling velocity necessary to explain the rate at which particles settle, under the assumption that the water column is well-mixed. This is expressed as

$$C(t) = C_0 e^{-(we/h)t},$$

where C(t) is the observed concentration ($g \cdot l^{-1}$) at time t (s), C_0 is the concentration ($g \cdot l^{-1}$) at time t=0, w_e is the effective clearance rate ($m \cdot s^{-1}$), and h is the SPM sample depth (m) (Curran *et al.,* 2004b). Clearance rates on the order of 0.1 $mm \cdot s^{-1}$ have been reported for high concentrations of flocculated fine sediment in the marine environment (Curran *et al.,* 2004b). In the wave tank, suspended particulate matter clearance rates ranged from 0.01 up to 0.1 $mm \cdot s^{-1}$. Mean values for non-dispersed and dispersed conditions (0.04 and 0.05 $mm \cdot s^{-1}$, respectively) show that dispersed particles clear the water column at a higher rate. This is supported by the high concentration of oil droplets at 35 cm depth identified in MVFC images immediately following dispersant application. In agreement with size versus settling relationships, clearance rates suggest that where sediment concentration is low and water temperature <10°C, dispersant use tends to be associated with faster-settling particles of a typically higher effective density. In contrast, the opportunity for the formation of larger, low-density flocs is increased in the absence of dispersant. This relation agrees well with MVFC-derived particle size distributions, which show particle growth through flocculation at the end of non-dispersed settling phases, and lends support to the argument that may dispersant impede particles' natural flocculation tendencies.

Laboratory-based settling velocity experiments revealed an increase in dilbit-derived OMA particle size and settling velocity associated with increased sediment concentration. At a sediment concentration of 50 mg L^{-1}, the average OMA particle size was 30% larger than that observed with 10 mg L^{-1} sediment concentration. Similar behaviour is typical of a fine sediment suspension, where particle sizes are influenced by rising concentration through increasing flocculation efficiency (Kranck 1981; Manning and Dyer, 2002). In addition, the settling velocity of OMA at 50 mg L^{-1} sediment concentration was >50% faster than that measured during the 10 mg L^{-1} condition. This compliments the notion that a high-concentration suspension produces large, inorganic flocs that settle rapidly (Kranck, 1980; Curran *et al.*, 2002).

The successful production of OMA in the lab, compared with the absence of OMA resulting from wave tank experiments, is owed to a number of factors. First, the time scale for OMA formation during wave tank experiments (1-2 hours) is much shorter than that provided to laboratory samples (16 to 24 hours). Such a limited time scale is likely to disadvantage OMA formation at low sediment concentration (Hill *et al.*, 2002). Second, the concentration of suspended material combined with oil in lab experiments (up to 100 mg L^{-1}) was greater than that explored during wave tank experiments (15-20 mg L^{-1}); higher sediment concentration increases the potential for inter-particle collisions and OMA formation, and also decreases the time necessary for formation (Sun *et al.*, 2013). Third, the organic content of suspended particulate in wave tank experiment water ranged from 50-80%, which represents a large amount of organic material for inorganic particles to interact with. This may have resulted in a depletion of fine particles that otherwise would have contributed to OMA formation. By comparison, the seawater used in lab-based experiments was filtered at a smaller pore size, and also was a much smaller volume, making filtering more effective. As a result, lab experiment water offered less organic material to interact with sediment particles, compared with that in the wave tank. The presence of organics to is known to impact the flocculation of inorganic particles (Kranck 1973; Sholkovitz, 1976), as sticky organic coatings increase the efficiency of floc formation (Eisma, 1986) and create slow-settling, loosely-packed flocs (Kranck and Milligan, 1991). Coupled with a low sediment concentration, wave tank experiments were most likely to produce these low-density, organic-rich flocs. Flocculation during lab experiments was dominated by large, inorganic flocs that tend to settle rapidly, due to the absence of organic material in experiment water. This role of organics in the flocculation process may have contributed to the discrepancy between lab and wave tank results as natural flocculation packaged inorganic particles in different ways. Finally, the level of kinetic mixing energy applied to disaggregate oil during lab experiments was greater than that produced by breaking waves in the wave tank. More energetic mixing likely allowed for the creation of a greater number of finer oil constituents in the laboratory situation, available to be coated with sediment and form OMA. Such a difference in turbulent energy dissipation between lab and wave tank experiments and the potential effects on OMA formation requires consideration and will be explored. As a result of these factors, while OMA has successfully been produced in the lab, OMA formation has not yet been replicated in larger-scale wave tank experiments. Future wave tank experiments will address this, namely by (1) extending the time-scale for mixing and settling phases to facilitate OMA production, (2) considering higher suspended sediment concentrations, and (3) making changes to the dispersant-to-oil ratio.

Additional lab experiments designed to determine the total petroleum hydrocarbons (TPH) in settled sediment, or the amount of oil incorporated with settled sediment, showed that more oil settled under conditions where higher sediment loads (50 & 100 mg L^{-1}) were combined with a lower concentration of dispersed oil (50 ppm). A substantial change in the amount of settled oil was associated with increased sediment concentration (from 10 to 50 mg L^{-1}), resulting in an increased percentage of TPH, from 5.1±2.2 % to 25.2±5.3 %. This supports the idea that, similar to flocculation, the efficiency of OMA formation increases with suspended sediment concentration, as has been demonstrated by studies where TPH sedimentation was found to be most efficient with sediment concentrations > 25 mg·l^{-1} (Khelifa *et al.*, 2008a,b; Ajijolaiya *et al.*, 2006; Sun *et al.*, 2010; Niu and Lee, 2013). However, in contrast with the results of these studies, results described here show that increasing the sediment load up to 100 mg L^{-1} may also be associated with a moderate reduction in the amount of settled oil. Results of lab experiments discussed here show that increasing the sediment load from 50 to 100 mg/L resulted in a 3.6% decrease in TPH sedimentation. Although this small decrease is essentially within the margin of error, it may suggest that a reduction in OMA formation efficiency can be linked to increasing sediment concentration. Further replication of this experiment will be pursued to elaborate on this result.

5.0 CONCLUSION

An initial series of wave tank experiments designed to study the particle behaviour of the in situ formation of diluted bitumen-derived OMA, and the influence of chemical dispersant (Corexit 9500) on the formation of OMA, has been completed. Overall, results suggest that in colder water (<10 °C) and at a low sediment concentration (~15 mg L^{-1}), in situ formation of OMA in the wave tank has been unsuccessful. This is contrary to lab studies, where dilbit-derived OMA formed using similar sediment concentration. Images from floc cameras demonstrated the efficiency of chemical dispersant in the wave tank but failed to capture the formation of OMA under the aforementioned conditions. An abrupt increase in particle size at 35 cm depth following the application of oil and dispersant has been attributed to dispersed oil being driven into the water column by wave energy. Particle size distributions remained relatively unchanged under non-dispersed conditions, until the volume of particles >100 µm began to increase as sediment particles flocculated in the final stages of the settling phase. It is noted that this did not occur during any experiment where dispersant was applied; this may represent an influence of dispersant on natural sediment flocculation, suggesting that it causes a decrease in aggregation efficiency. Results describing particle size and settling velocity of OMA developed from laboratory studies reinforce the established notion that OMA formation increases with suspended sediment concentration. Mean per-experiment settling velocity measurements were generally lower than in situ floc settling rates discussed in literature, and wave tank results cover a large range that compares well with floc settling rates from high-concentration flood plumes. However, this is likely due to the aggregation of inorganic grains in the wave tank.

ACKNOWLEDGEMENTS

This research was supported by the World Class Tanker Safety (WCTS) fund from Fisheries and Oceans Canada. Thanks is given to COOGER staff for wave tank operations and preparing samples for laboratory experiments.

REFERENCES

Ajijolaiya, L.O., Hill, P.S., Khelifa, A., Islam, R.M., Lee, K. (2006). Laboratory investigation of the effects of mineral size and concentration on the formation of oil–mineral aggregates. Marine Pollution Bulletin 52: 920–927.

Curran, K.J., Hill, P.S., Milligan, T.G. (2002). Fine-grained suspended sediment dynamics in the Eel river flood plume. Continental Shelf Research 22: 2537-2550.

Curran,K.J., Hill,P.S., Schell,T.M., Milligan,T.G., Piper,D.J.W. (2004a). Inferring the mass fraction of floc deposited mud: application to fine-grained turbidites. Sedimentology 51 (5): 927–944.

Curran, K.J., T.G. Milligan, G. Bugden, B. Law, and M. Scotney. (2004b). Suspended Sediment, Water Quality, and Hydrodynamics of the Petitcodiac River Estuary, New Brunswick (2002–2003). Can. Tech. Rep. Fish. Aquat. Sci. 2516: xi + 88 p.

Curran, K.J., Hill, P.S., Milligan, T.G., Mikkelsen, O.A., Law, B.A., Durrieu de Madron, X., Bourrin, F. (2007). Settling velocity, effective density, and mass composition of suspended sediment in a coastal bottom boundary layer, Gulf of Lions, France. Continental Shelf Research 27: 1408–1421.

Eisma, D. (1986). Flocculation and de-flocculation of suspended matter in estuaries. Netherlands Journal of Sea Research 20(2): 183-199.

Fox, J.M., Hill, P.S., Milligan, T.G., Boldrin, A. (2004). Flocculation and sedimentation on the Po River Delta. Marine Geology 203: 95–107.

Fu, J., Gong, Y., Zhao, X., O'Reilly, S.E., Zhao, D. (2014). Effects of oil and dispersant on formation of marine oil snow and transport of oil hydrocarbons. Environ. Sci. Technol. 48: 14392-14399.

Gong, Y., Zhao, X., Cai, Z., O'Reilly, S.E., Hao, X., Zhao, D. (2014). A review of oil, dispersed oil and sediment interactions in the aquatic environment: Influence on the fate, transport and remediation of oil spills. Marine Pollution Bulletin 79: 16–33.

Government of Canada. (2013). Federal Government Technical Report: Properties, composition and marine spill behaviour, fate and transport of two diluted bitumen products from the Canadian oil sands. pp. 1–85, ISBN 978-1-100-23004-7 Cat. No.: En84-96/2013E-PDF.

Hill, P. S., Milligan, T. G., Geyer, W. R. (2000). Controls on effective settling velocity of suspended sediment in the Eel River flood plume. Continental Shelf Research 20 (16): 2095-2111.

Hill, P.S., Khelifa, A., Lee, K. (2002). Time scale for oil droplet stabilization by mineral particles in turbulent suspensions. Spill Science & Technology Bulletin 8 (1): 73–81.

Khelifa, A., Stoffyn-Egli, P., Hill, P.S., Lee, K. (2002). Characteristics of oil droplets stabilized by mineral particles: effects of oil type and temperature. Spill Science & Technology Bulletin 8 (1): 19-30.

Khelifa, A., Hill, P.S., Lee, K. (2005). Assessment of minimum sediment concentration for OMA formation using a Monte Carlo model, In: Al-Azab, M., El-Shorbagy, W., Al-Ghais, S. (Eds.), Oil Pollution and its Environmental Impact in the Arabian Gulf Region. Elsevier, pp. 93–104.

Khelifa, A., Fieldhouse, B., Wang, Z., Yang, M., Landriault, M., Fingas, C.E., Brown, C.E., Gamble, L. (2007). A Laboratory Study on formation of Oil-SPM aggregates using the NIST standard reference material 1941b, In: Proceeding of the Thirtieth Arctic and marine Oil Spill Program Technical Seminar, Environment Canada, Ottawa, ON: pp. 35–48.

Khelifa, A., Chun, M., Eubank, J.L.E., Brown, C.E. (2008a). Physical properties of oil-SPM aggregates: experiments with the NIST standard reference material 1941b, In: Proceedings of the 31st AMOP technical seminar on environmental contamination and response, Environment Canada, Ottawa, ON: Vol. 1, pp. 35–51.

Khelifa, A., Fingas, M., Brown, C. (2008b). Effects of Dispersants on Oil-SPM Aggregation and Fate in US Coastal Waters: Final Report Submitted to The Coastal Response Research Center, March 2008, pp. 57.

King, T.L., Robinson, B., Boufadel, M., Lee, K. (2014). Flume tank studies to elucidate the fate and behavior of diluted bitumen spilled at sea. Mar. Pollut. Bull. (2014), http://dx.doi.org/10.1016/j.marpolbul.2014.04.042

King, T., Robinson, B., Ryan, S., Lu, Y., Zhou, Q., Ju, L., Li, J., Sun, P., Lee, K. (2015). Fate of Chinese and Canadian Oils Treated with Dispersants in a Wave Tank. Proceedings of the Thirty-Eighth AMOP Technical Seminar on Environmental Contamination and Response, Environment Canada, Ottawa, ON, 798-811.

Kranck, K. (1973). Flocculation of suspended Sediment in the Sea. Nature 246: 348-350.

Kranck, K., Milligan, T. (1979). The use of the Coulter Counter in studies of particle size-distributions in aquatic environments. Bedford Institute of Oceanography.

Kranck, K., Milligan, T. (1980). Experiments on the significance of flocculation in the settling of fine-grained sediment in still water. Can. J. Earth Sci.17 (11): 1517–1526.

Kranck, K. (1981). Particulate matter grain-size characteristics and flocculation in a partially-mixed estuary. Sedimentology 28: 107-114.

Kranck, K., Milligan, T.G. (1985). Origin of Grain Size Spectra of Suspension Deposited Sediment. Geo-Marine Letters 5: 61-66

Kranck, K., Milligan, T.G. (1991). Grain Size in Oceanography. In: Syvitski, J.P.M. (Ed.), Principles, Methods, and Applications of Particle Size Analysis. Cambridge University Press, NewYork, pp. 368.

Kranck, K., Milligan, T.G. (1992). Characteristics of suspended particles at an 11 hour anchor station in San Francisco Bay, California. Journal of Geophysical Research 97 (C7): 11,373–11,382.

Kranck, K., Smith, P., Milligan, T.G. (1996a). Grain-size characteristics of fine-grained unflocculated sediments I: 'one-round' distributions. Sedimentology 43: 589–596.

Kranck, K., Smith,P., Milligan,T.G. (1996b). Grain-size characteristics of fine-grained unflocculated sediments II: 'multi-round' distributions. Sedimentology 43: 597–606.

Law, B. A., Hill, P. S., Milligan, T. G., Curran, K. J., Wiberg, P. L., & Wheatcroft, R. A. (2008). Size sorting of fine-grained sediments during erosion: results from the western Gulf of Lions. Continental Shelf Research, 28(15), 1935-1946.

Law, B.A., Milligan, T.G., Hill, P.S., Newgard, J., Wheatcroft, R.A., Wiberg, P.L. (2012). Flocculation on a muddy intertidal flat in Willapa Bay, Washington, Part I: A regional survey of the grain size of surficial sediments. Continental Shelf Research 28 (15): 1935-1946.

Lee, K., Stoffyn-Egli, P., Tremblay, G.H., Owens, E.H., Sergy, G.A., Guénette, C.C., Prince, R.C. (2003). Oil–Mineral Aggregate Formation on Oiled Beaches: Natural

Attenuation and Sediment Relocation. Spill Science & Technology Bulletin, Vol. 8, (3): 285–296.

Lee, K., Li, Z., King, T., Kepkay, P., Boufadel, M.C., Venosa, A.D., Mullin, J.V. (2008). Effects of chemical dispersants and mineral fines on partitioning of petroleum hydrocarbons in natural seawater. In: International Oil Spill Conference 2008, No. 1: 633–638.

Lee, K., Bugden, J., Cobanli, S., King, T., McIntyre, C., Robinson, B., Ryan, S., Wohlgeschaffen, G. (2012). UV-Epifluorescence Microscopy Analysis of Sediments Recovered from the Kalamazoo River. US EPA Kalamazoo Administrative Record. Document, 1277.

Li, Z., Kepkay, P., Lee, K., King, T., Boufadel, M.C., Venosa, A.D. (2007). Effects of chemical dispersants and mineral fines on crude oil dispersion in a wave tank under breaking waves. Marine Pollution Bulletin 54: 983–993.

Li, Z., Lee, K., King, T., Boufadel, M.C., Venosa, A.D. (2008). Assessment of chemical dispersant effectiveness in a wave tank under regular non-breaking and breaking wave conditions. Marine Pollution Bulletin 56: 903–912.

Lindstrom, J.E., Braddock, J.F. (2002). Biodegradation of petroleum hydrocarbons at low temperature in the presence of the dispersant Corexit 9500. Marine Pollution Bulletin 44: 739–747.

Macdonald, R.W (Ed.). (1983). The distribution and dynamics of suspended particles in Kitimat fjord system. Can. Tech. Rep. Hydrogr. Ocean Sci. 18,116-137.

Manning, A. J., & Dyer, K. R. (2002). A comparison of floc properties observed during neap and spring tidal conditions. Proceedings in Marine Science, 5, 233-250.

McCave, I. N. (1984). Size spectra and aggregation of suspended particles in the deep ocean. Deep Sea Research Part A. Oceanographic Research Papers, 31(4), 329-352.

Mikkelsen, O.A., Milligan, T.G., Hill, P.S., Moffat, D. (2004). INSSECT—an instrumented platform for investigating floc properties close to the seabed. Limnology and Oceanography Methods 2: 226-236.

Mikkelsen, O.A., Milligan, T.G., Hill, P.S., Chant, R.J., Jago, C.F., Jones, S.E., Krivtsov, V., Mitchelson-Jacob, G. (2007). The influence of schlieren on in situ optical measurements used for particle characterization. Limnology and Oceanography Methods 6 (3): 133-143.

Milligan, T. G., and Kranck, K. (1991). Electroresistance particle size analyzers. In: Principles, methods and applications of particle size analysis. Cambridge University Press, New York (1991): 109-118.

Milligan, T. G., & Law, B. A. (2005). The effect of marine aquaculture on fine sediment dynamics in coastal inlets. In: Environmental Effects of Marine Finfish Aquaculture (239-251). Springer Berlin Heidelberg.

Milligan, T. G., Hill, P. S., & Law, B. A. (2007). Flocculation and the loss of sediment from the Po River plume. Continental Shelf Research, 27(3), 309-321.

Niu, H., Li, Z., K., Lee, K., Kepkay, P., Mullin, J.V. (2011). Modelling the Transport of oil-mineral aggregates (OMAs) in the Marine Environment and Assessment of Their Potential Risks. Environmental Modelling and Assessment 16 (1): 61-75.

Niu, H., Lee, K. (2013). Study of the dispersion/settling of oil-mineral-aggregates using particle tracking model and assessment of their potential risks. Int. J. Environment and Pollution (52): 32–51.

Page, C.A., Bonner, J.S., Sumner, P.L., McDonald, T.J., Autenrieth, R.L., Fuller, C.B. (2000). Behaviour of a chemically dispersed oil and a whole oil on a nearshore environment. Wat. Res. 34 (9): 2507-2516.

Sholkovitz, E.R. (1976). Flocculation of dissolved organic and inorganic matter during the mixing of river water and seawater. Geochlmica et Cosmochnnica Acta 40: 831-845.

Singer, M. M., George, S., Jacobson, S., Lee, I., Weetman, L. L., Tjeerdema, R. S., & Sowby, M. L. (1996). Comparison of acute aquatic effects of the oil dispersant Corexit 9500 with those of other Corexit series dispersants. Ecotoxicology and Environmental Safety 35(2): 183-189.

Sørensen, L., Melbye, A.G., Booth, A.M. (2014). Oil droplet interaction with suspended sediment in the seawater column: Influence of physical parameters and chemical dispersants. Marine Pollution Bulletin 78: 146-152.

Sternberg, R.W., Berhane, I., Ogston, A.S. (1999). Measurement of size and settling velocity of suspended aggregates on the northern California continental shelf. Marine Geology 154: 43-53.

Sun, J., Khelifa, A., Zheng, X., Wang, Z., So, L.L., Wong, S., Yang, C., Fieldhouse, B. (2010). A laboratory study on the kinetics of the formations of oil-suspended particulate matter aggregates using the NIST-1941b sediment. Marine Pollution Bulletin 60: 1701-1707.

Sun, J., Zhao, D., Zhao, C., Liu, F., Zheng, X. (2013). Investigation of the kinetics of oil–suspended particulate matter aggregation. Marine Pollution Bulletin 76: 250–257.

Sun, J., Khelifa, A., Zhao, C., Zhao, D., Wang, Z. (2014). Laboratory investigation of oil–suspended particulate matter aggregation under different mixing conditions. Science of the Total Environment 473–474: 742–749.

Venosa, A.D., King, D.W., and Sorial, G.A. (2002). The Baffled Flask Test for Dispersant Effectiveness: A Round Robin Evaluation of Reproducibility and Repeatability. Spill Science and Technology Bulletin, 7 (5-6):299-308.

Venosa, A.D., Holder, E.L. (2007). Biodegradability of dispersed crude oil at two different temperatures. Marine Pollution Bulletin 54: 545–553.

Wang, W., Zheng, Y., Li, Z., Lee, K. (2011). PIV investigation of oil- mineral interaction for an oil spill application. Chemical Engineering Journal 170 (1): 241-249.

Wang, W., Zheng, Y., Lee, K. (2013). Role of the hydrophobicity of mineral fines in the formation of oil-mineral aggregates. Canadian Journal for Chemical Engineering 91: 698-703.

Zhang, H., Khatibi, M., Zheng, Y., Lee, K., Li, Z., Mullin, J.V. 2010. Investigation of OMA formation and the effect of minerals. Marine Pollution Bulletin 60: 1433–1441.

FIGURES AND TABLES

Table 1: Summary of data collection

Summary of data collection in the wave tank (2014), describing experimental conditions (S = sediment only; S,O = sediment and oil; S,O,D = sediment, oil and dispersant), successful data collection, and the number of water samples drawn from the tank to monitor concentration.

Expt.	Date	Condition	MVFC	SVS-MVFC	ADCP/OBS	LISST1387	H_2O (# samples)
WTE-1	15-Apr-14	S	YES	NO	YES	NO	29
WTE-2	23-Apr-14	S, O	NO	YES	YES	YES	35
WTE-3	30-Apr-14	S, O, D	YES	NO	YES	YES	72
WTE-4	07-May-14	S, O	YES	YES	YES	YES	68
WTE-5	21-May-14	S, O, D	YES	YES	YES	YES	72
WTE-6	27-May-14	S, O	NO	YES	YES	YES	71
WTE-7	29-May-14	S, O	YES	YES	YES	YES	68
WTE-8	03-Jun-14	S, O	YES	YES	YES	YES	70
WTE-9	05-Jun-14	S, O, D	YES	YES	YES	YES	70
WTE-10	10-Jun-14	S, O, D	YES	YES	YES	YES	64
WTE-11	12-Jun-14	S, O, D	YES	YES	YES	YES	70
WTE-12	19-Jun-14	S, O	YES	YES	YES	YES	70
WTE-13	24-Jun-14	S, O, D	YES	YES	YES	YES	69
WTE-14	18-Jul-14	S	NO	YES	YES	NO	68
WTE-15	07-Oct-14	S, O, D	YES	YES	YES	YES	69
WTE-16	02-Oct-14	S, O	NO	YES	YES	YES	67
WTE-17	09-Oct-14	S, O, D	YES	YES	YES	YES	69
WTE-18	14-Oct-14	S, O	YES	YES	YES	YES	67
WTE-19	16-Oct-14	S, O, D	YES	YES	YES	YES	68
WTE-20	22-Oct-14	S, O	YES	YES	YES	YES	68

Table 2: Experimental parameters.

Summary of experimental parameters during wave tank experiments (2014), including the temperature (°C) and salinity (ppt) of experiment water. The type of sediment used is identified by the site it was collected from (DC-09 or DC-26), and the amount (g) used was dependant on the water content of the recovered sediment. The type (AWB or CLB) and amount (g) of diluted bitumen product is also indicated.

Expt.	Date	H_2O temp. (°C)	Salinity (ppt)	Sediment		Oil	
				Source	Amount (g)	Type	Amount (g)
WTE-1	15-Apr-14	6.1	26.7	DC-09	-	-	-
WTE-2	23-Apr-14	5.9	28.5	DC-09	839.0	AWB	237.9
WTE-3	30-Apr-14	4.0	28.5	DC-09	841.0	AWB	215.4
WTE-4	07-May-14	6.0	29.7	DC-26	1521.0	CLB	245.3
WTE-5	21-May-14	9.0	30.0	DC-09	840.1	AWB	241.7
WTE-6	27-May-14	7.0	29.7	DC-26	1525.3	CLB	231.7
WTE-7	29-May-14	7.5	30.3	DC-09	841.7	AWB	261.4
WTE-8	03-Jun-14	10.2	29.6	DC-09	841.7	AWB	236.5
WTE-9	05-Jun-14	10.2	30.3	DC-26	1526.4	CLB	245.4
WTE-10	10-Jun-14	9.6	30.4	DC-09	840.1	AWB	249.7
WTE-11	12-Jun-14	12.9	30.2	DC-26	1528.0	CLB	235.7
WTE-12	19-Jun-14	11.5	29.1	DC-26	1518.9	CLB	238.3
WTE-13	24-Jun-14	13.1	29.6	DC-26	1523.3	CLB	252.2
WTE-14	18-Jul-14	15.7	28.0	DC-26	1530.0	-	-
WTE-15	07-Oct-14	13.8	30.2	DC-26	1387.0	AWB	223.1
WTE-16	02-Oct-14	14.2	28.1	DC-26	1387.0	AWB	223.7
WTE-17	09-Oct-14	12.1	30.7	DC-26	1396.0	AWB	238.8
WTE-18	14-Oct-14	13.2	31.1	DC-26	1390.0	AWB	229.9
WTE-19	16-Oct-14	14.0	30.8	DC-26	1388.0	AWB	245.4
WTE-20	22-Oct-14	13.2	31.3	DC-26	1389.0	AWB	227.1

Table 3: Reported experiments

Summary and description of wave tank experiments summarized in this report. These have been grouped into non-dispersed and dispersed categories, based on the presence or absence of chemical dispersant.

Experiment	Conditions	Water Temp. (°C)	Salinity (PPT)	Background SPM (mg L^{-1})	Background Organics (%)
WTE-4	Non-Dispersed, < 10 °C	6.0	29.7	0.96	83
WTE-7	Non-Dispersed, < 10 °C	7.5	30.3	1.00	70
WTE-8	Non-Dispersed, < 10 °C	10.2	29.6	1.84	66
WTE-12	Non-Dispersed, < 10 °C	11.5	29.1	2.41	57
WTE-3	Dispersed,< 10 °C	4.0	28.5	1.76	58
WTE-5	Dispersed,< 10 °C	9.0	30.0	1.64	58
WTE-9	Dispersed,< 10 °C	10.2	30.3	2.24	54
WTE-10	Dispersed,< 10 °C	9.6	30.4	2.46	63

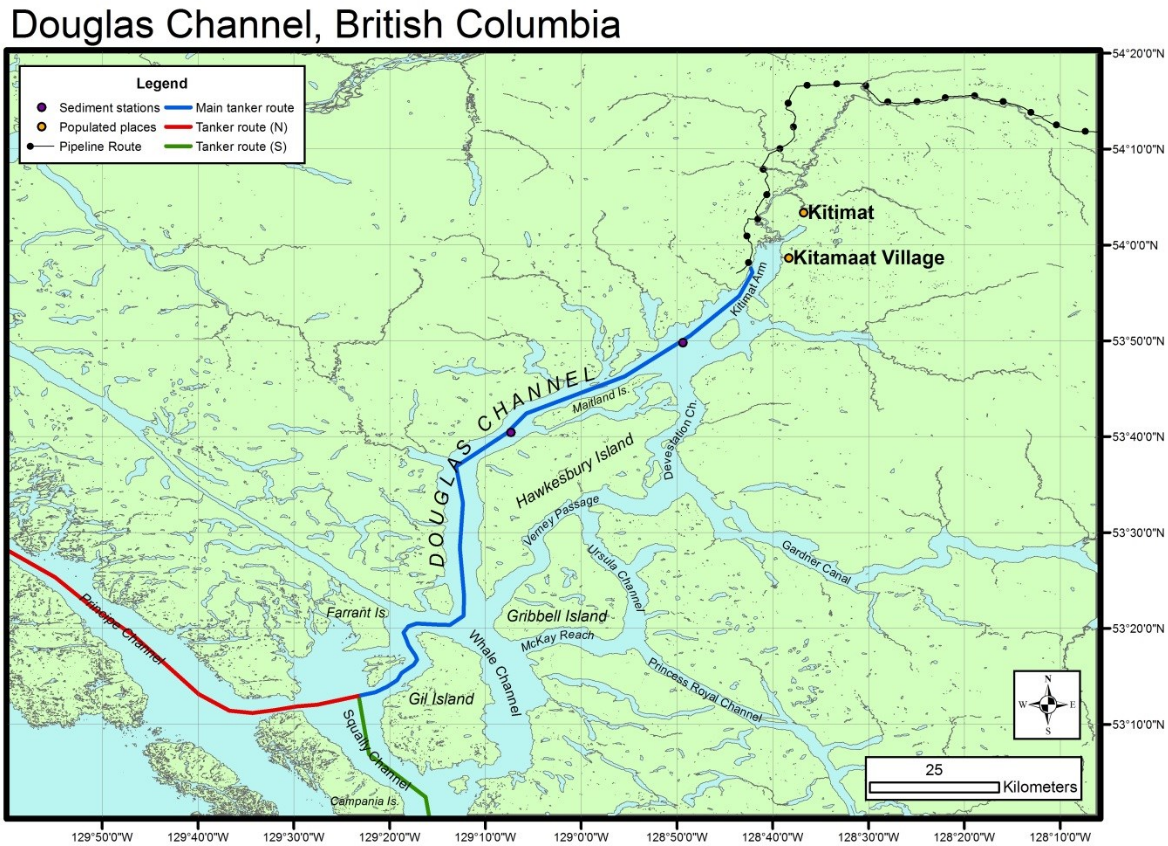

Figure 1: Douglas Channel region

Map depicting Douglas Channel and the surrounding region. Sediment source locations are shown (purple dots), along with the proposed tanker route through Douglas Channel (blue line), and the northern (red line) and southern (green line) approaches through Principe and Squally channels.

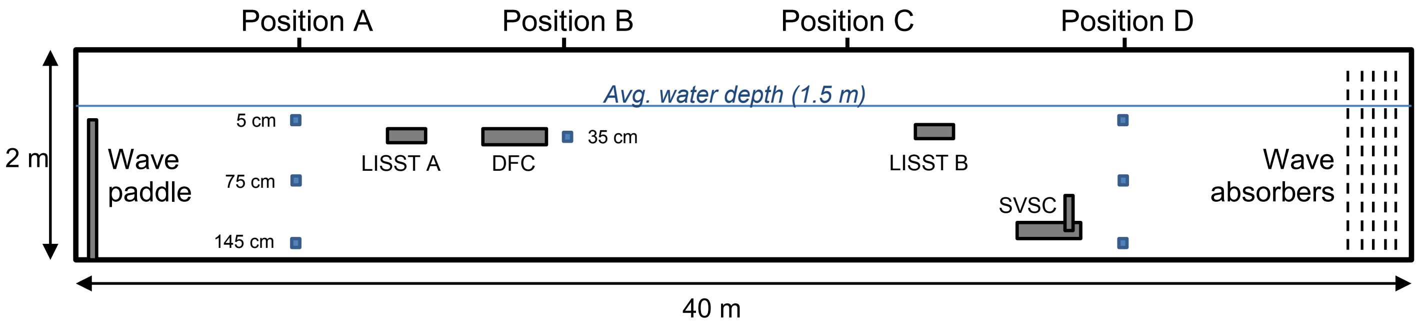

Figure 2: Wave tank schematic

Illustration of the wave tank, showing general dimensions, instrument locations (rectangles with labels), and water sampling positions (top axis) and depths (small squares). The wave-generating paddle and wave absorbers are shown at opposite ends of the wave tank.

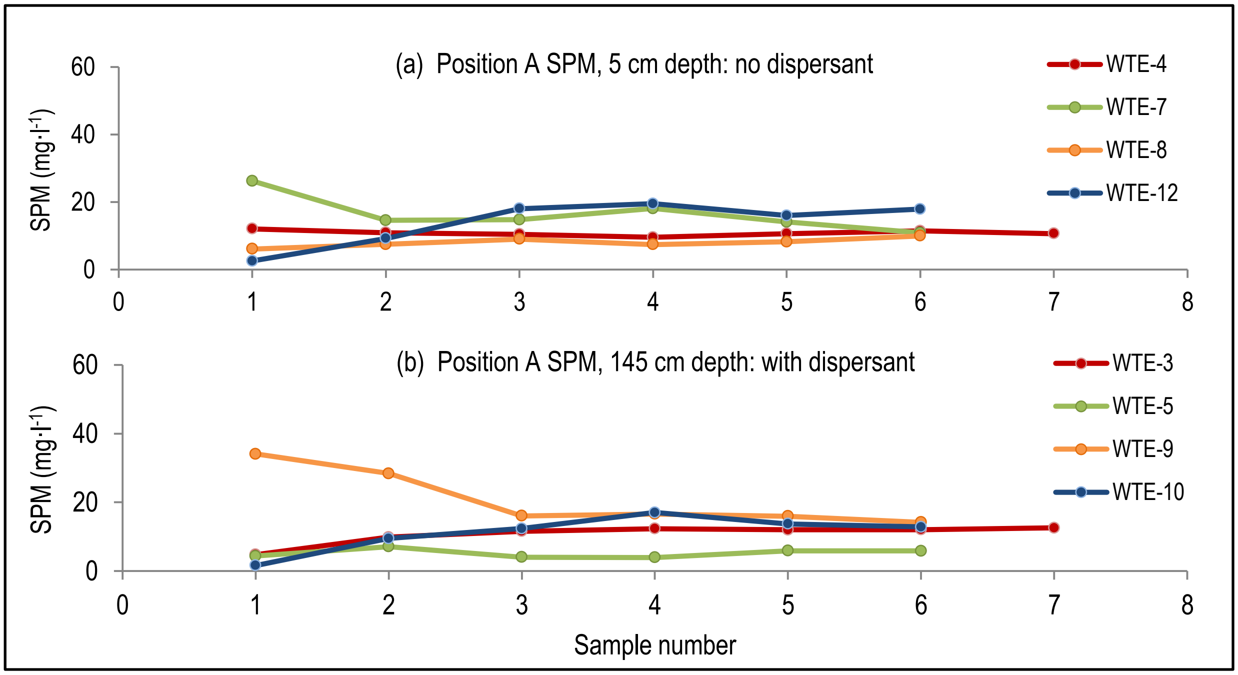

Figure 3: Position 'A' SPM

The concentration of suspended particulate matter (SPM) ($mg \cdot l^{-1}$) at position A (near the wave-generating paddle) at (a) 5 and (b) 145 cm depth, through both mixing phases. Non-dispersed experiments are shown in the top panel, while dispersed experiments are shown in the bottom panel.

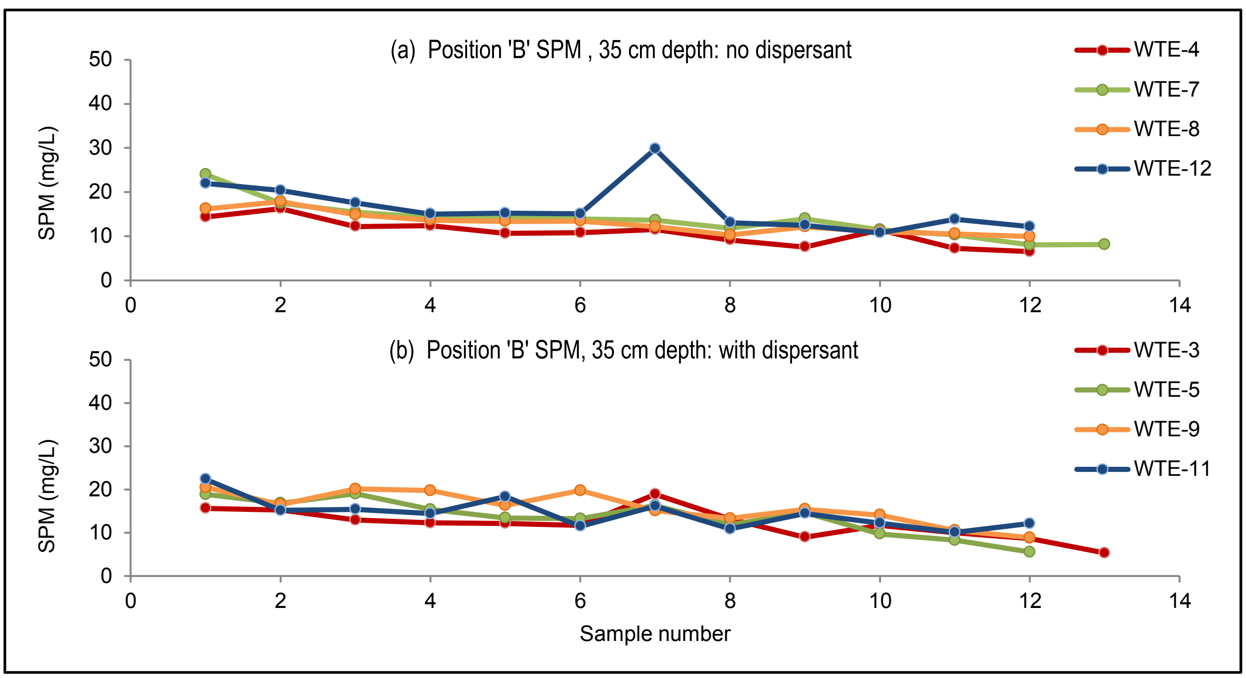

Figure 4: Position 'B' SPM

The concentration of suspended particulate matter (SPM) ($mg \cdot l^{-1}$) at position B (near the MVFC) at (a) 5 and (b) 145 cm depth, through all phases. Non-dispersed experiments are shown in the top panel, while dispersed experiments are shown in the bottom panel.

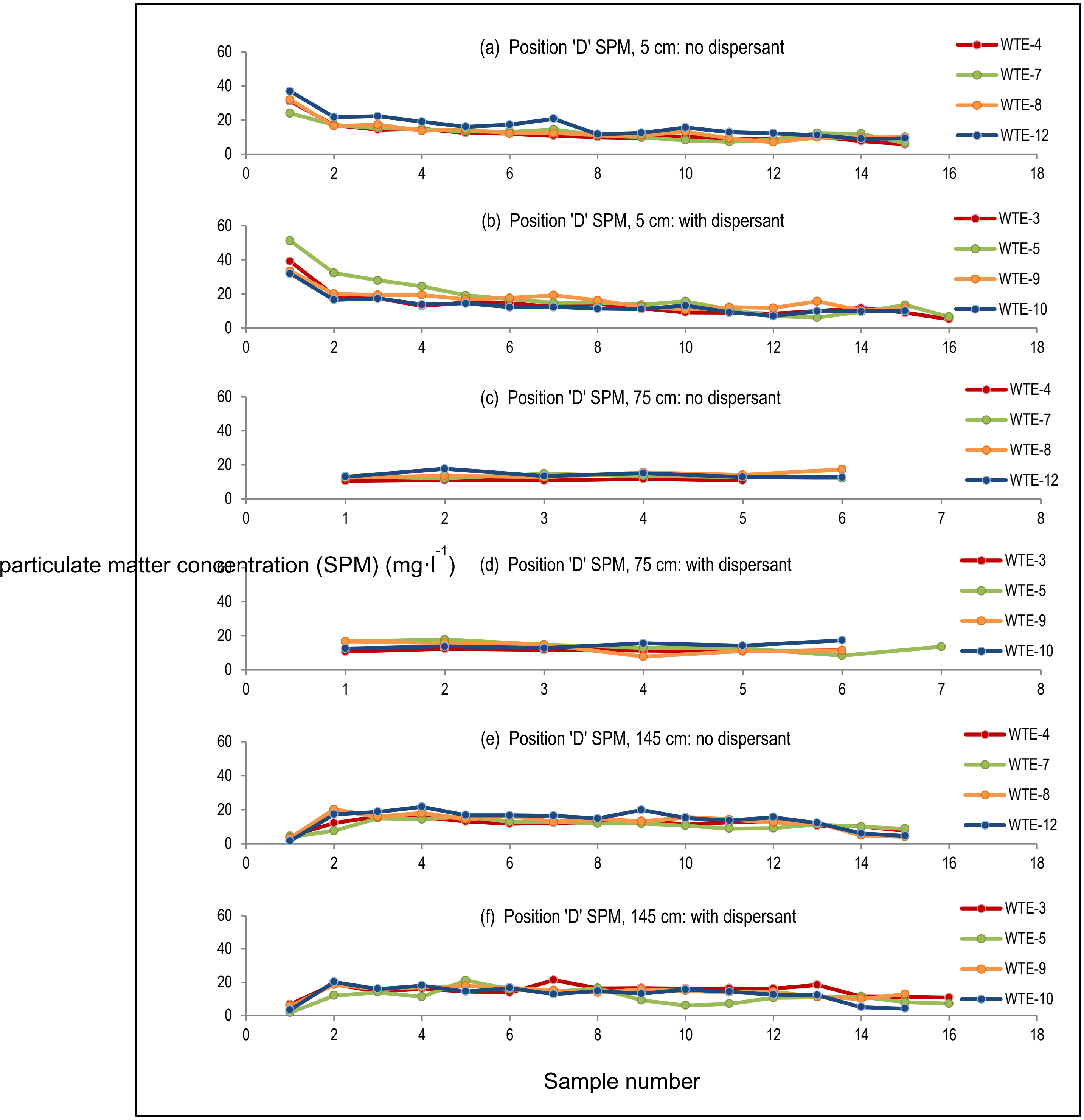

Figure 5: Position 'D' SPM

The concentration of suspended particulate matter (SPM) (mg·l^{-1}) at position D (near the SVS-MVFC) at 5, 75 and 145 cm depth, through all phases. Non-dispersed experiments are shown in panels a, c and e, while dispersed experiments are shown in panels b, d and f.

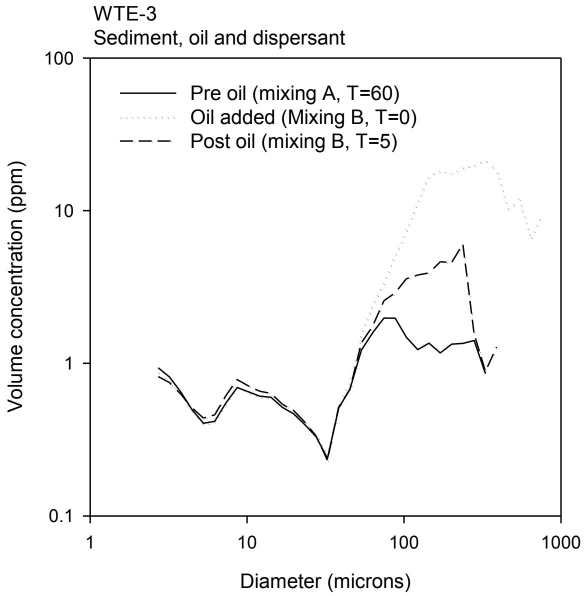

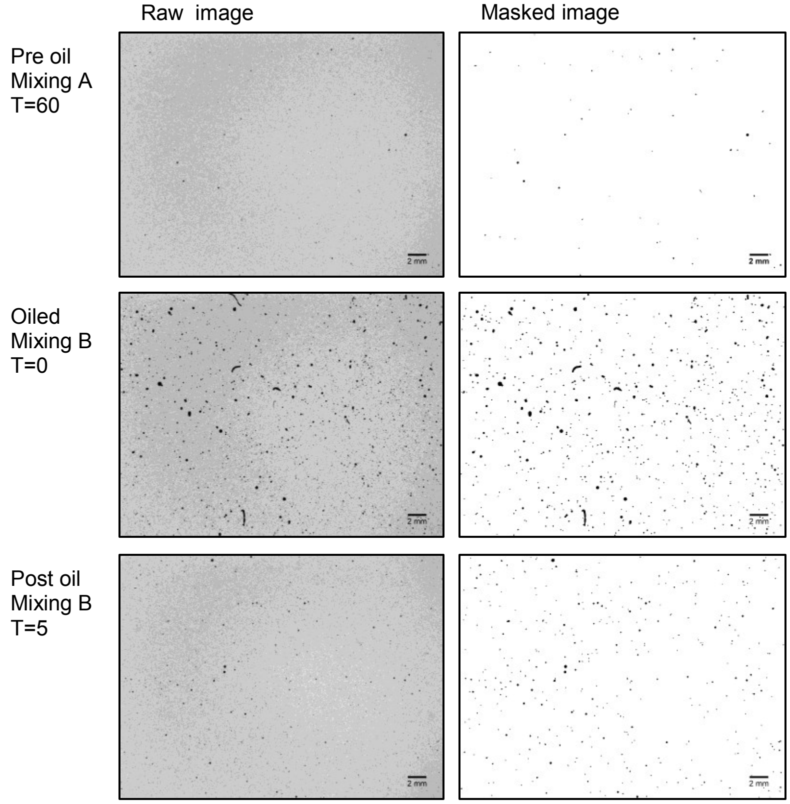

Figure 6: Wave tank experiment 3 combined sediment, oil and dispersant at a water temperature of 4.0°C, with a salinity of 28.5 ppt. Log-log plots of merged volume concentration (ppm) versus particle diameter (microns) from the floc camera and LISST are shown, along with raw and masked images from the floc camera, for pre-oil, oil added, and post-oil conditions.

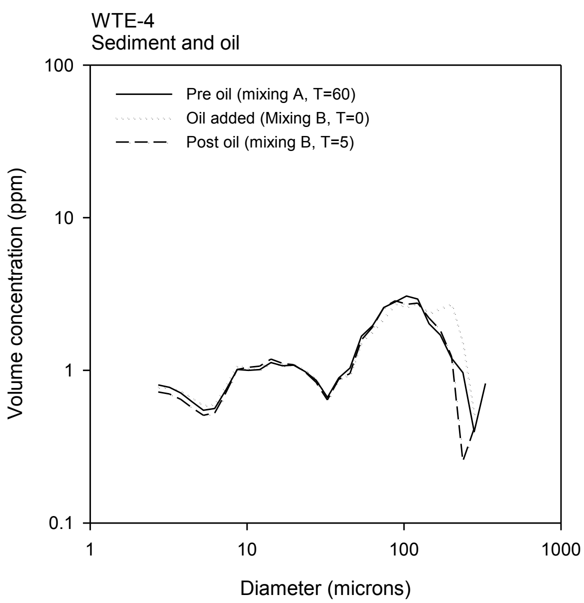

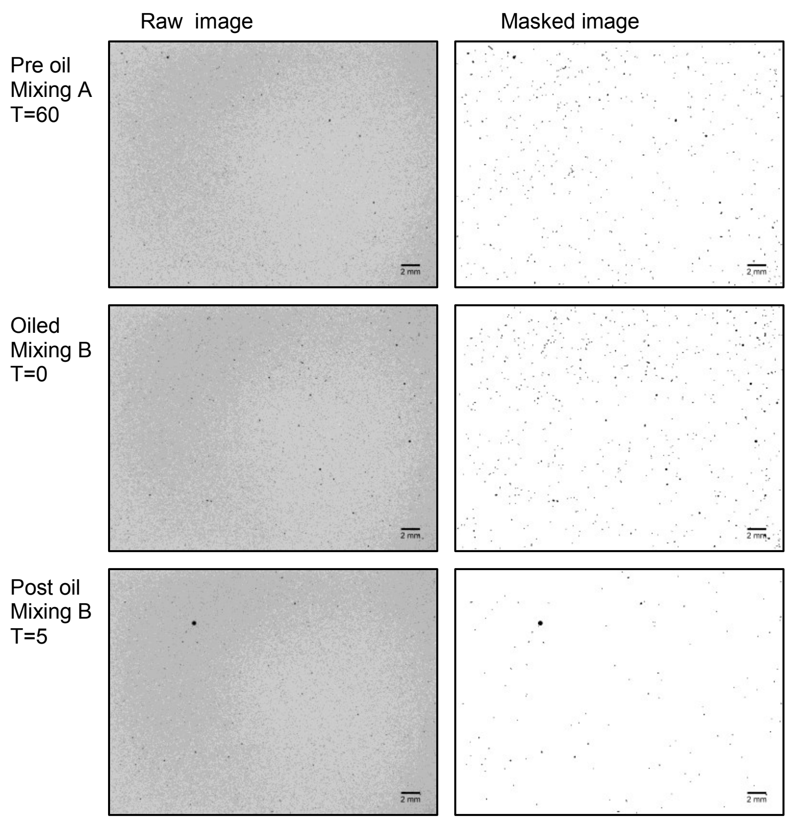

Figure 7: Wave tank experiment 4 combined sediment and oil at a water temperature of 6.0°C, with a salinity of 29.7 ppt. Log-log plots of merged volume concentration (ppm) versus particle diameter (microns) from the floc camera and LISST are shown, along with raw and masked images from the floc camera, for pre-oil, oil added, and post-oil conditions.

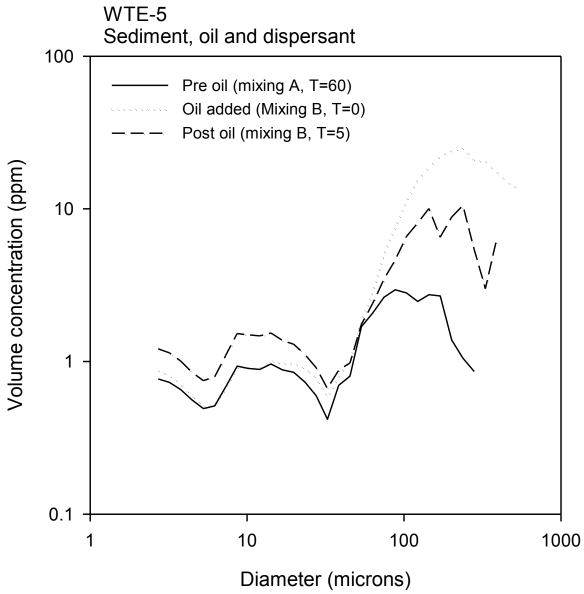

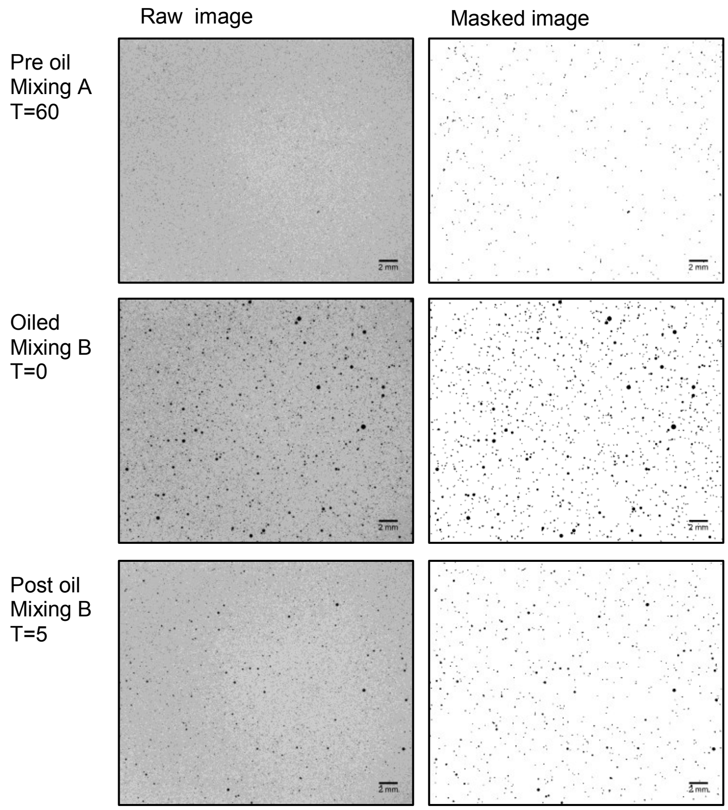

Figure 8: Wave tank experiment 5 combined sediment, oil and dispersant at a water temperature of 9.0°C, with a salinity of 30.0 ppt. Log-log plots of merged volume concentration (ppm) versus particle diameter (microns) from the floc camera and LISST are shown, along with raw and masked images from the floc camera, for pre-oil, oil added, and post-oil conditions.

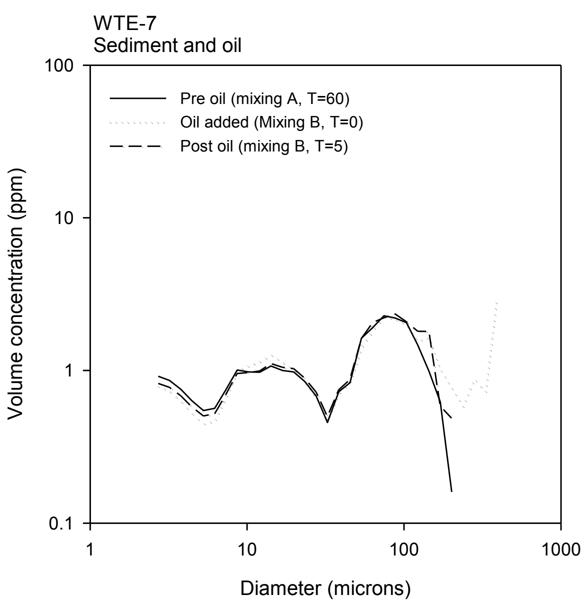

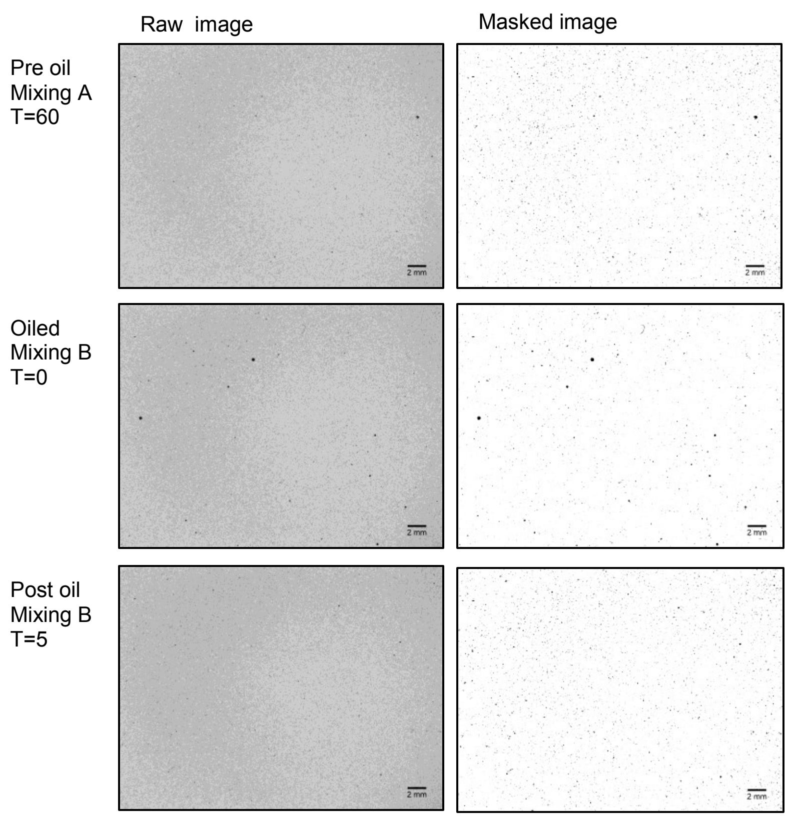

Figure 9: Wave tank experiment 7 combined sediment and oil at a water temperature of 7.5°C, with a salinity of 30.3 ppt. Log-log plots of merged volume concentration (ppm) versus particle diameter (microns) from the floc camera and LISST are shown, along with raw and masked images from the floc camera, for pre-oil, oil added, and post-oil conditions.

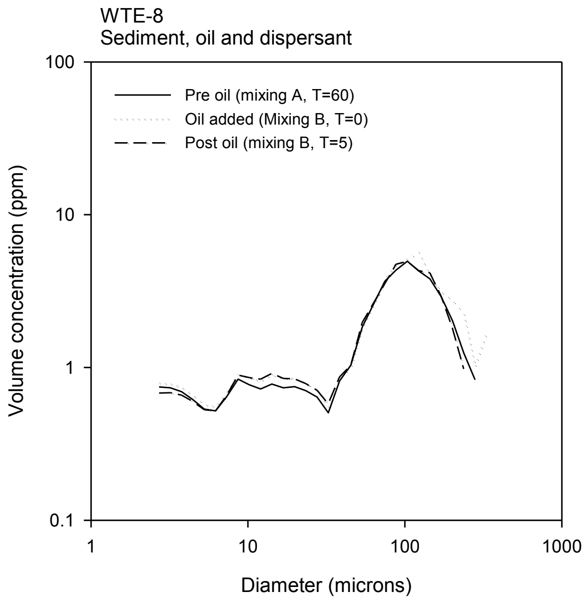

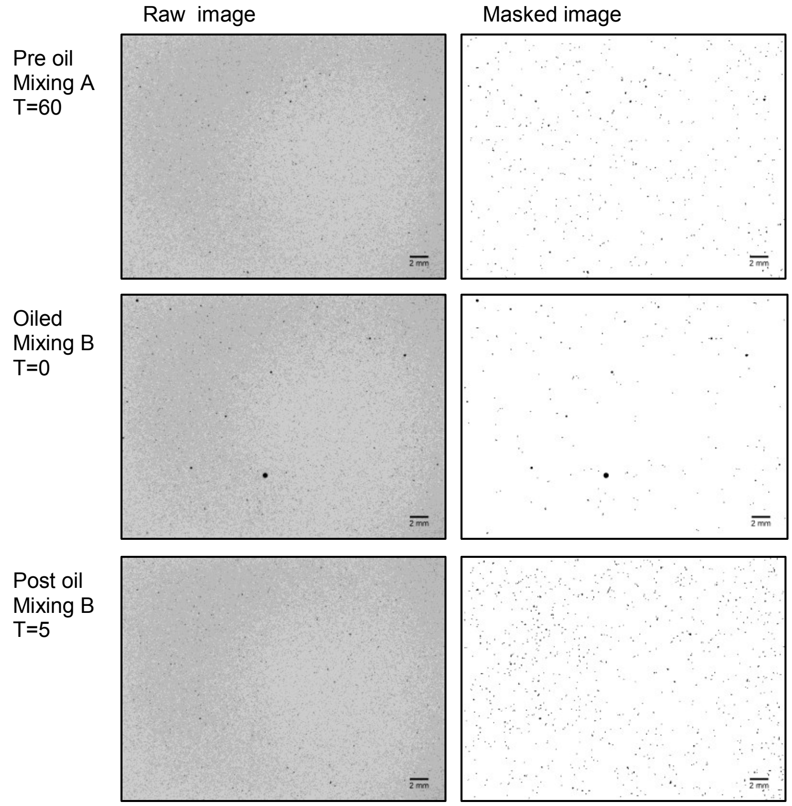

Figure 10: Wave tank experiment 8 combined sediment and oil at a water temperature of 10.2°C, with a salinity of 29.6 ppt. Log-log plots of merged volume concentration (ppm) versus particle diameter (microns) from the floc camera and LISST are shown, along with raw and masked images from the floc camera, for pre-oil, oil added, and post-oil conditions.

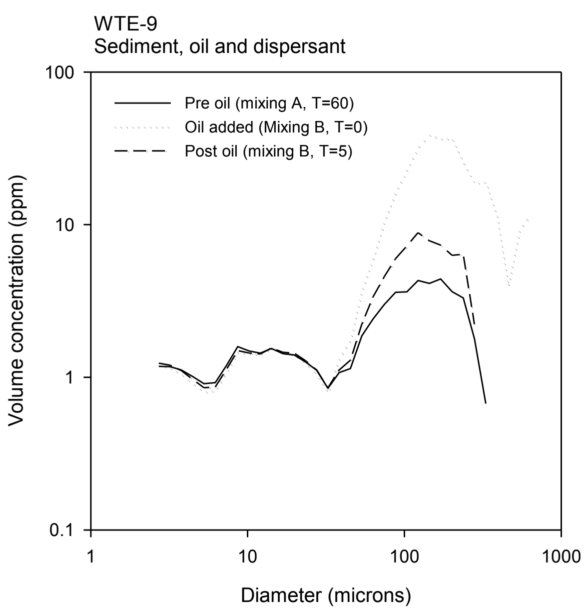

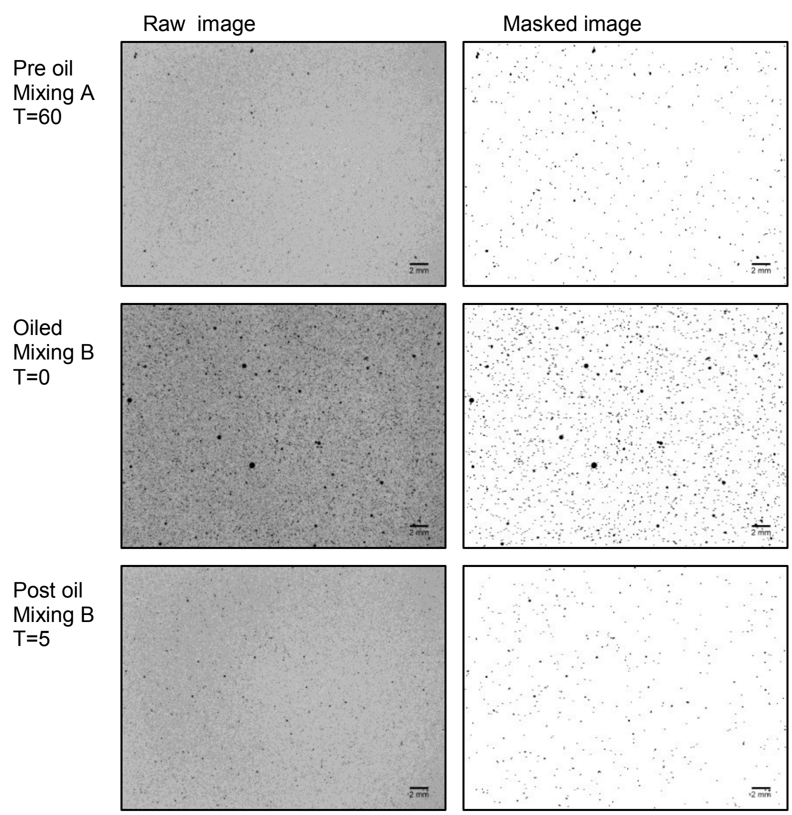

Figure 11: Wave tank experiment 9 combined sediment, oil and dispersant at a water temperature of 10.2°C, with a salinity of 30.3 ppt. Log-log plots of merged volume concentration (ppm) versus particle diameter (microns) from the floc camera and LISST are shown, along with raw and masked images from the floc camera, for pre-oil, oil added, and post-oil conditions.

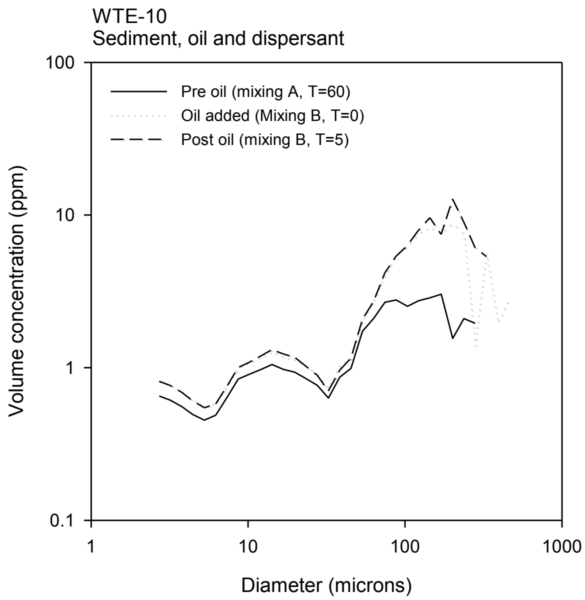

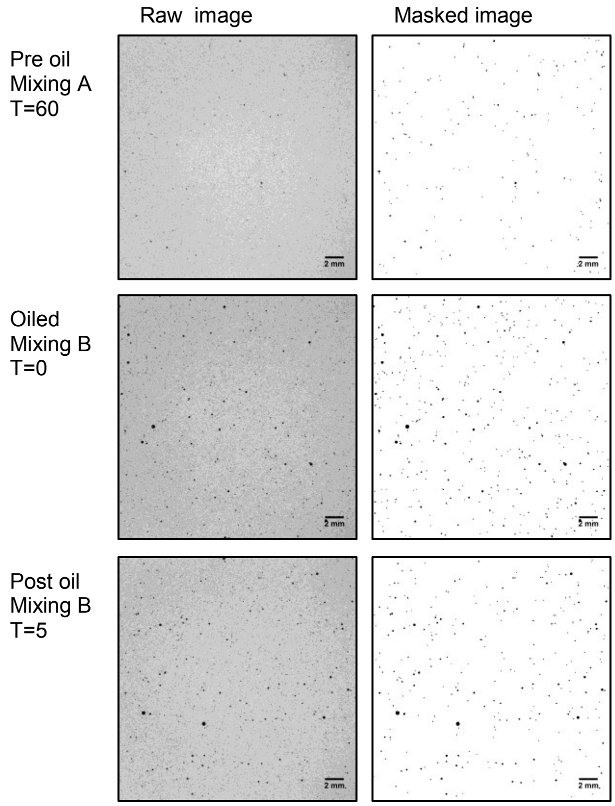

Figure 12: Wave tank experiment 10 combined sediment, oil and dispersant at a water temperature of 9.6°C, with a salinity of 30.4 ppt. Log-log plots of merged volume concentration (ppm) versus particle diameter (microns) from the floc camera and LISST are shown, along with raw and masked images from the floc camera, for pre-oil, oil added, and post-oil conditions. WTE-10 images were cropped to exclude obstruction on the lens, resulting in smaller images.

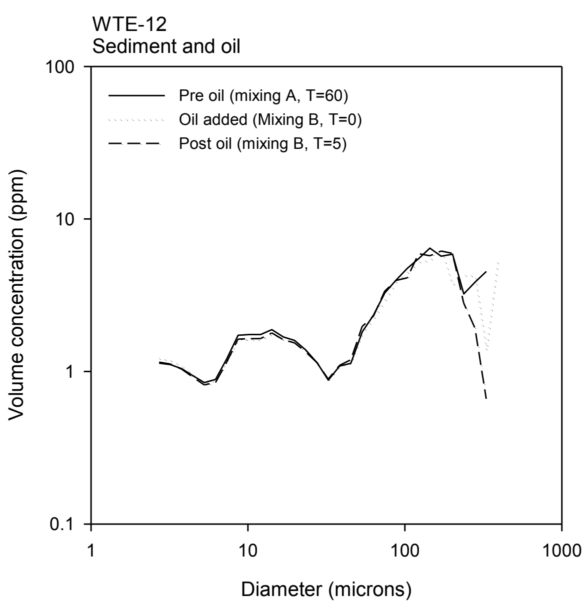

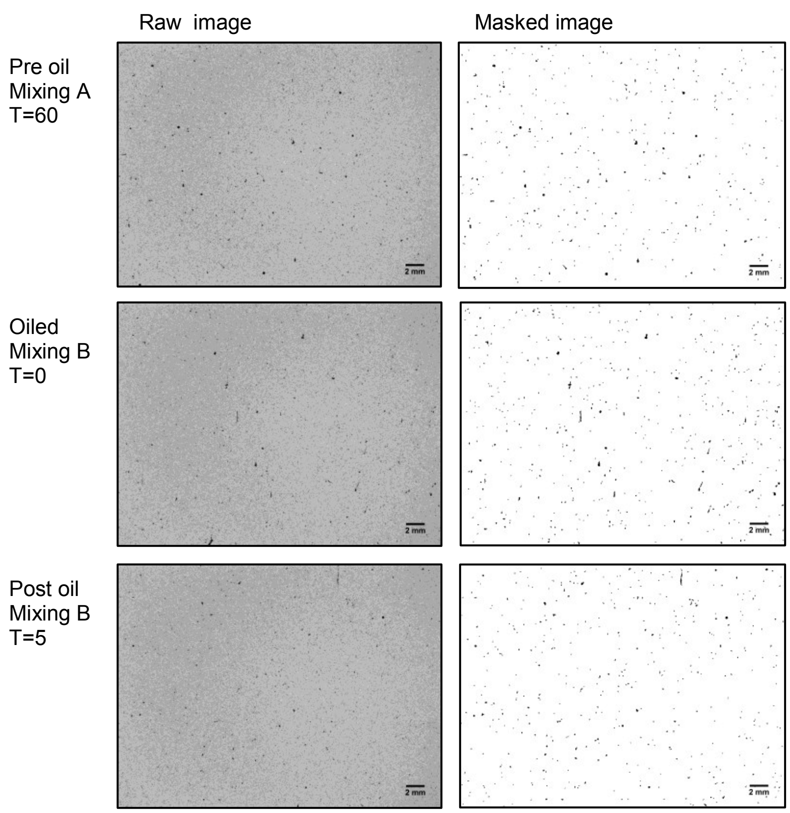

Figure 13: Wave tank experiment 12 combined sediment and oil at a water temperature of 11.5°C, with a salinity of 29.1 ppt. Log-log plots of volume concentration (ppm) versus particle diameter (microns) from the floc camera and LISST are shown, along with raw and masked images from the floc camera, for pre-oil, oil added, and post-oil conditions.

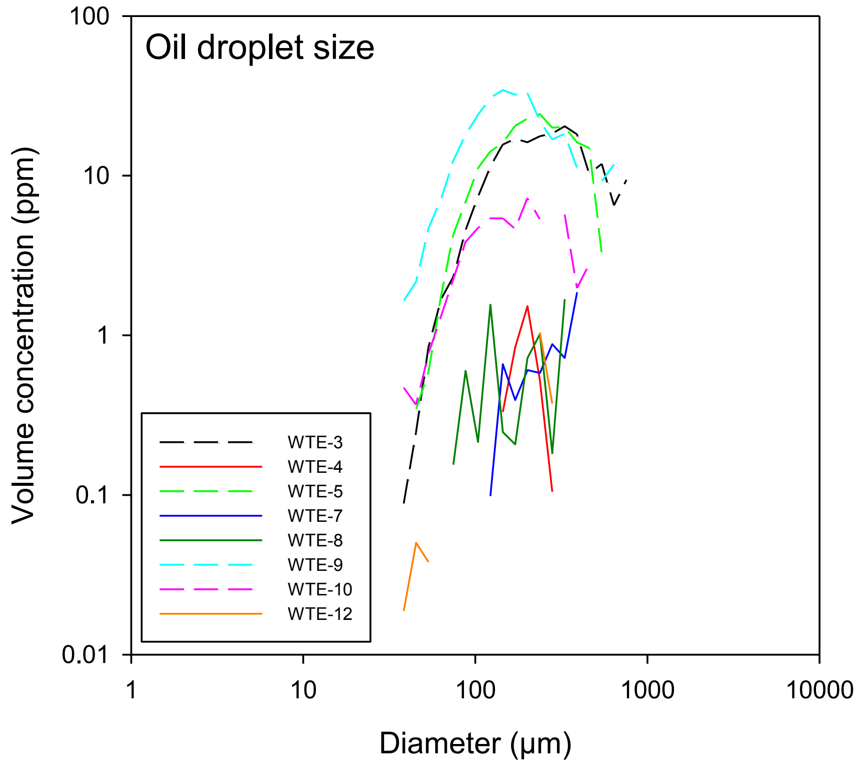

Figure 14: Oil droplet sizes

Droplet sizes at 35 cm depth were determined via subtraction of post-oil merged grain size spectra from pre-oil merged grain size spectra, the difference of which represents the size of suspended oil droplets. Above, volume concentration (ppm) is plotted against particle diameter for dispersed conditions (dashed lines) and non-dispersed conditions (solid lines).

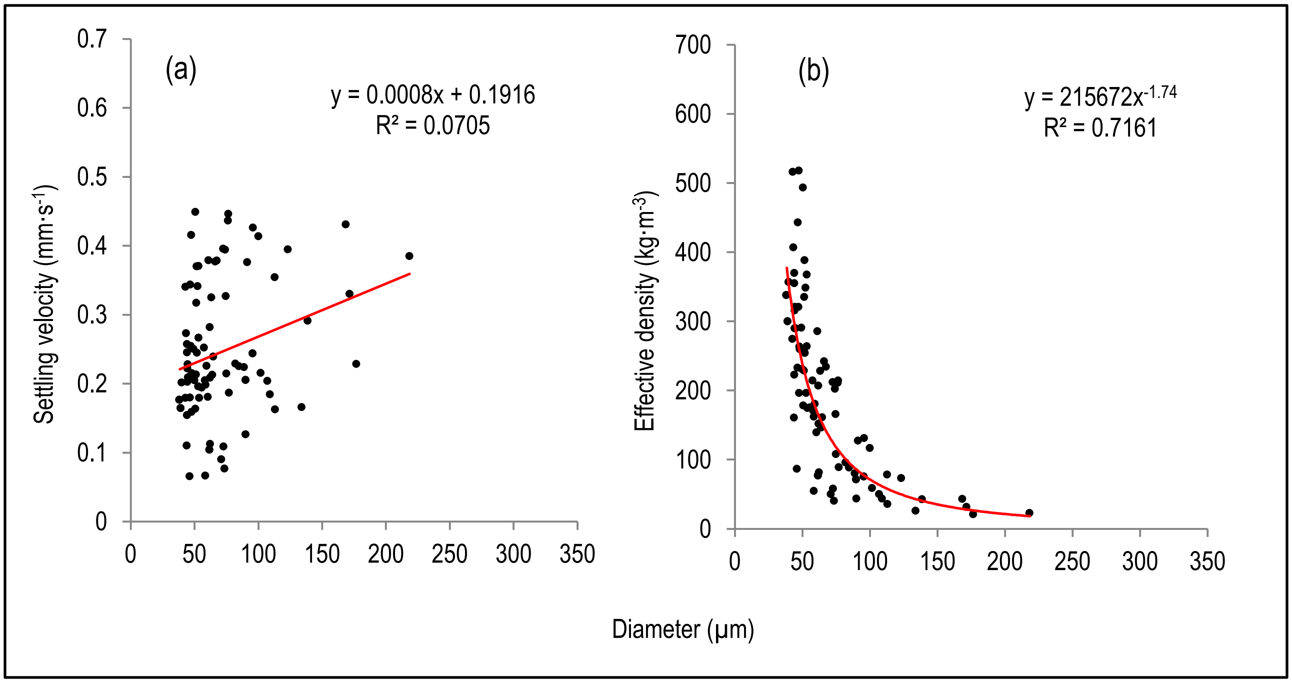

Figure 15: Size versus settling and effective density relationships, WTE-4

Settling velocity ($mm \cdot s^{-1}$) and effective particle density ($kg \cdot m^{-3}$) results for non-dispersed conditions, from wave tank experiment 4. Effective particle density describes the density of particles less that of seawater (1020 $g \cdot cm^{-3}$). Data are plotted as settling velocity or effective density versus particle diameter (µm) and are fitted to (a) linear and (b) power law models.

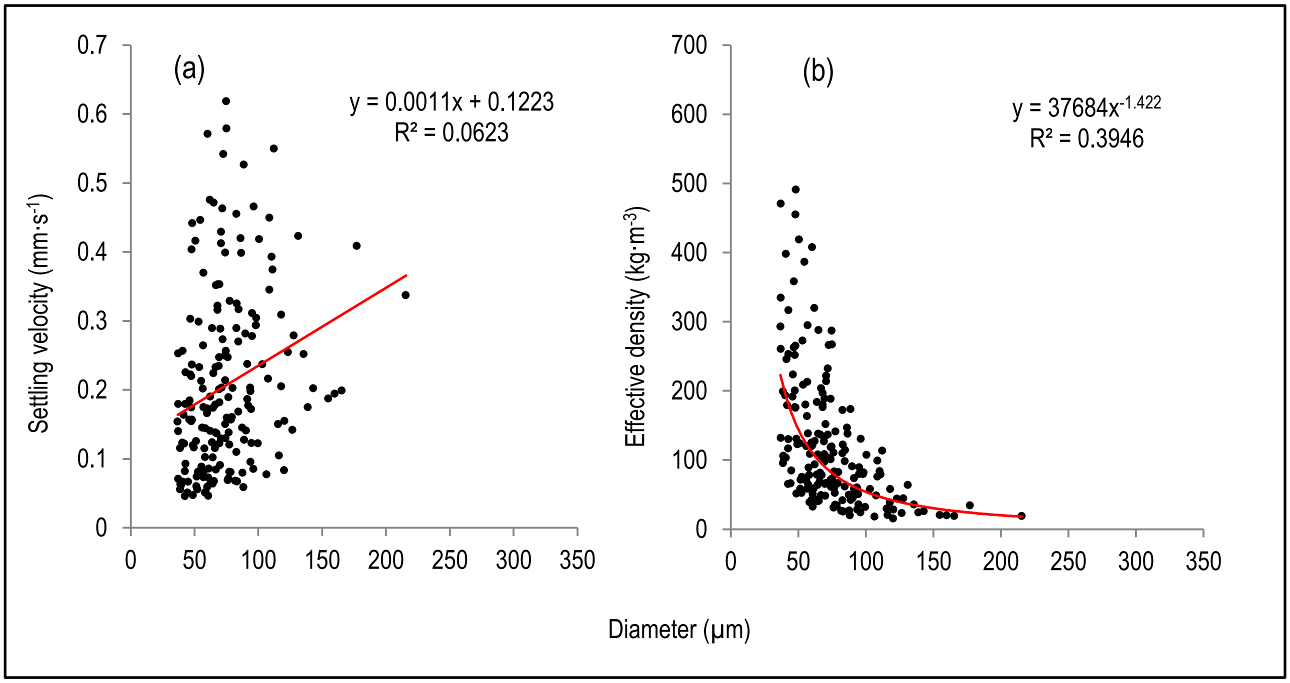

Figure 16: Size versus settling and effective density relationships, WTE-5

Settling velocity ($mm \cdot s^{-1}$) and effective particle density ($kg \cdot m^{-3}$) results for dispersed conditions, from wave tank experiment 5. Effective particle density describes the density of particles less that of seawater (1020 $g \cdot cm^{-3}$). Data are plotted as settling velocity or effective density versus particle diameter (µm) and are fitted to (a) linear and (b) power law models.

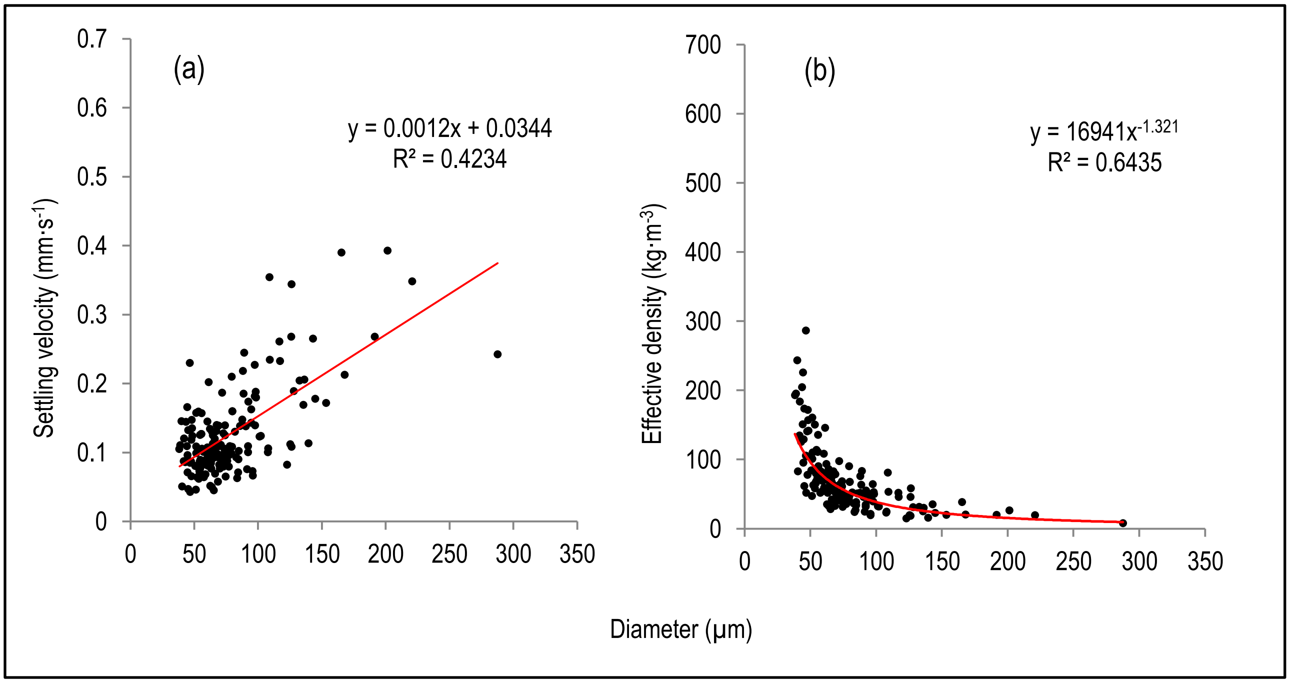

Figure 17: Size versus settling and effective density relationships, WTE-7

Settling velocity ($mm \cdot s^{-1}$) and effective particle density ($kg \cdot m^{-3}$) results for non- dispersed conditions, from wave tank experiment 7. Effective particle density describes the density of particles less that of seawater (1020 $g \cdot cm^{-3}$). Data are plotted as settling velocity or effective density versus particle diameter (µm) and are fitted to (a) linear and (b) power law models.

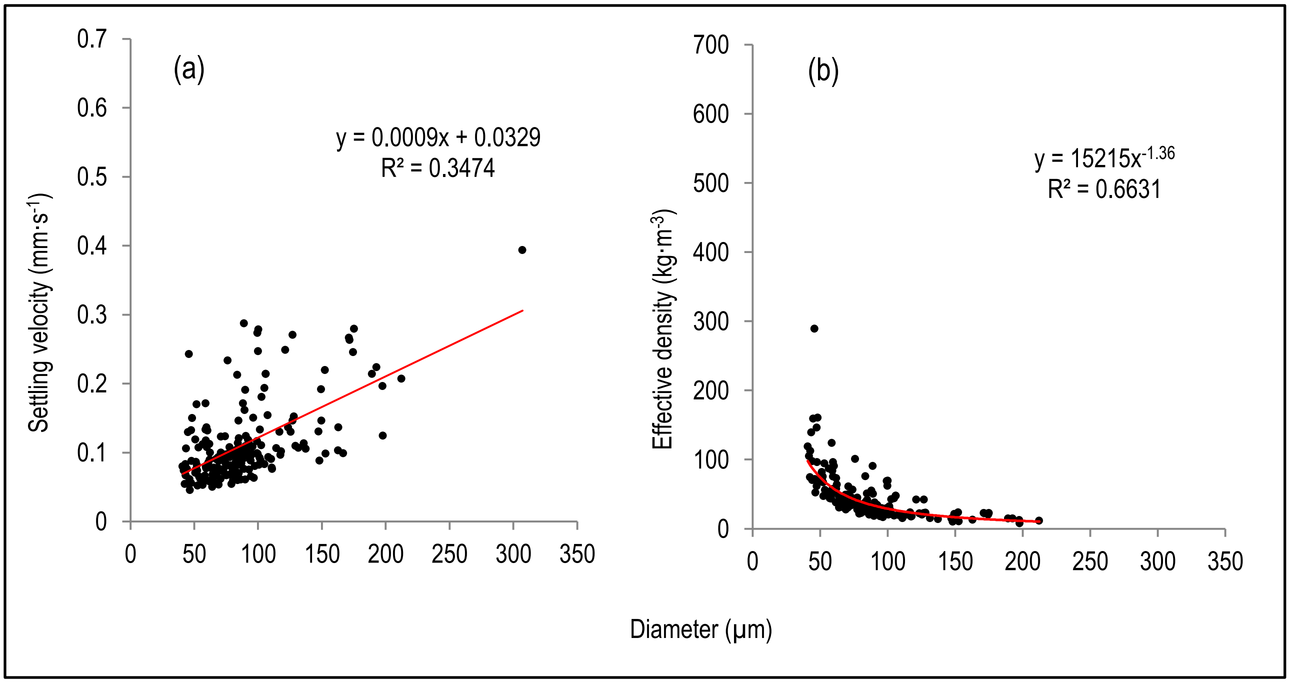

Figure 18: Size versus settling and effective density relationships, WTE-8

Settling velocity ($mm \cdot s^{-1}$) and effective particle density ($kg \cdot m^{-3}$) results for non- dispersed conditions, from wave tank experiment 8. Effective particle density describes the density of particles less that of seawater (1020 $g \cdot cm^{-3}$). Data are plotted as settling velocity or effective density versus particle diameter (µm) and are fitted to (a) linear and (b) power law models.

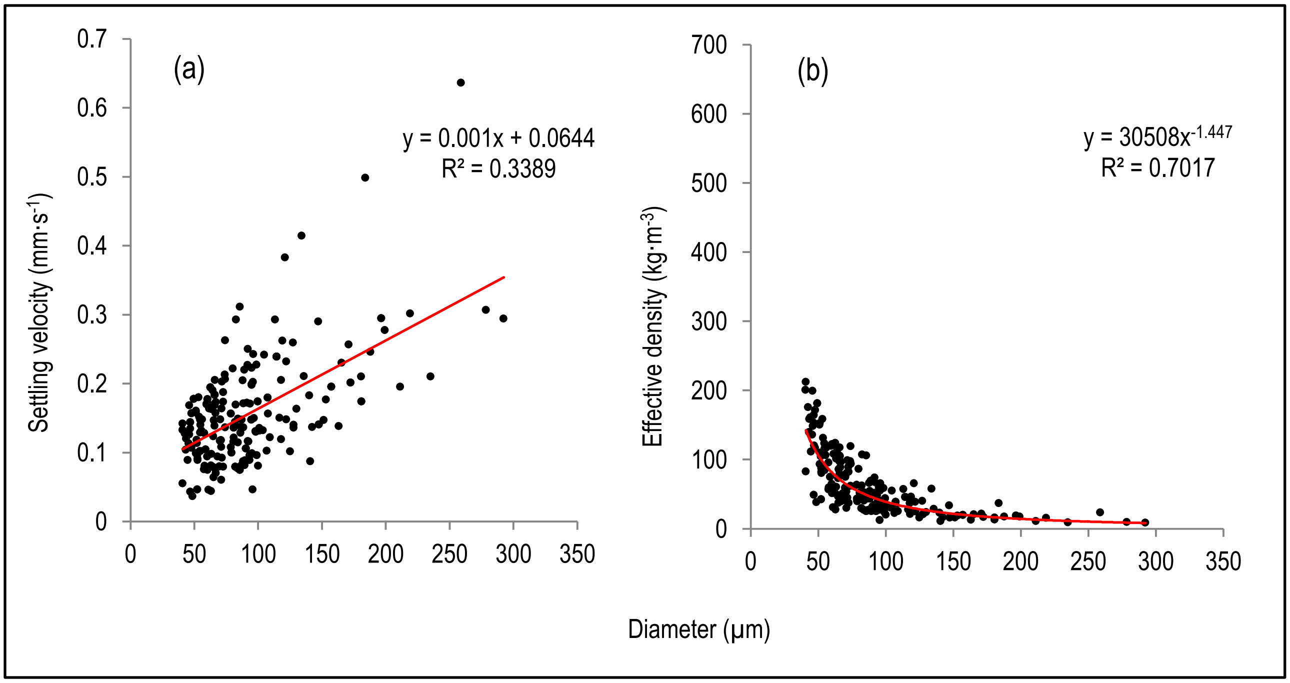

Figure 19: Size versus settling and effective density relationships, WTE 9

Settling velocity ($mm \cdot s^{-1}$) and effective particle density ($kg \cdot m^{-3}$) results for dispersed conditions, from wave tank experiment 9. Effective particle density describes the density of particles less that of seawater (1020 $g \cdot cm^{-3}$). Data are plotted as settling velocity or effective density versus particle diameter (µm) and are fitted to (a) linear and (b) power law models.

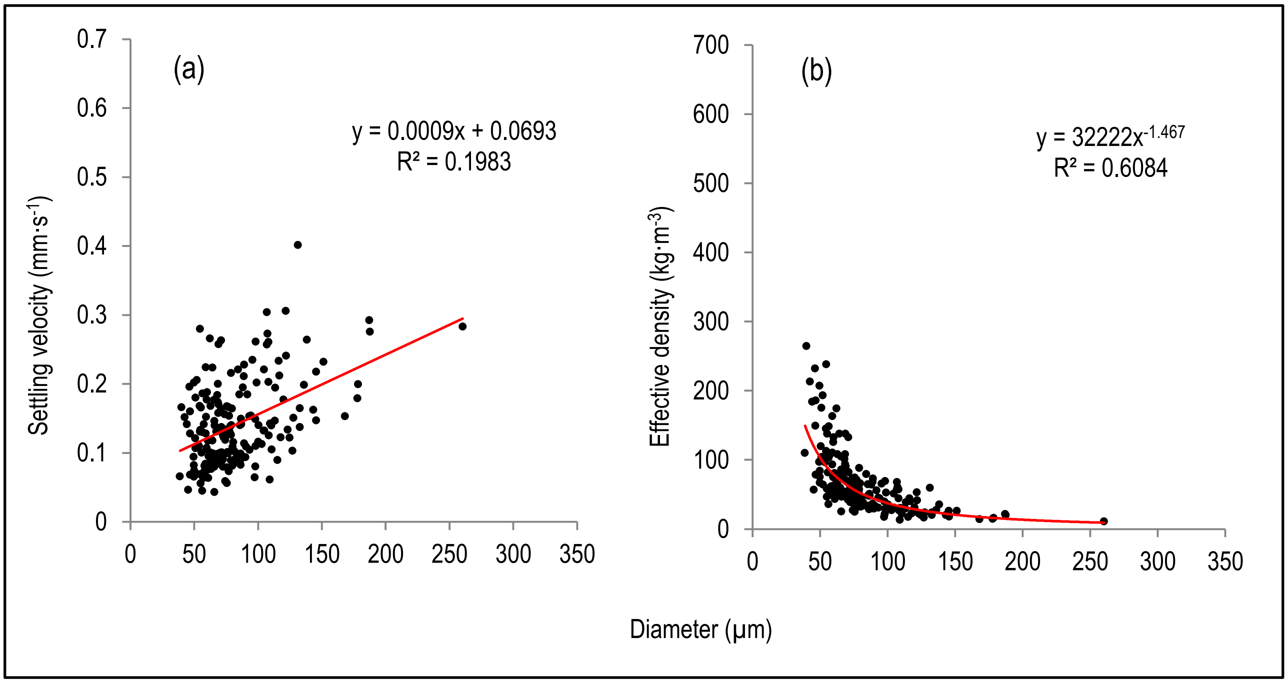

Figure 20: Size versus settling and effective density relationships, WTE 10

Settling velocity ($mm \cdot s^{-1}$) and effective particle density ($kg \cdot m^{-3}$) results for dispersed conditions, from wave tank experiment 10. Effective particle density describes the density of particles less that of seawater (1020 $g \cdot cm^{-3}$). Data are plotted as settling velocity or effective density versus particle diameter (µm) and are fitted to (a) linear and (b) power law models.

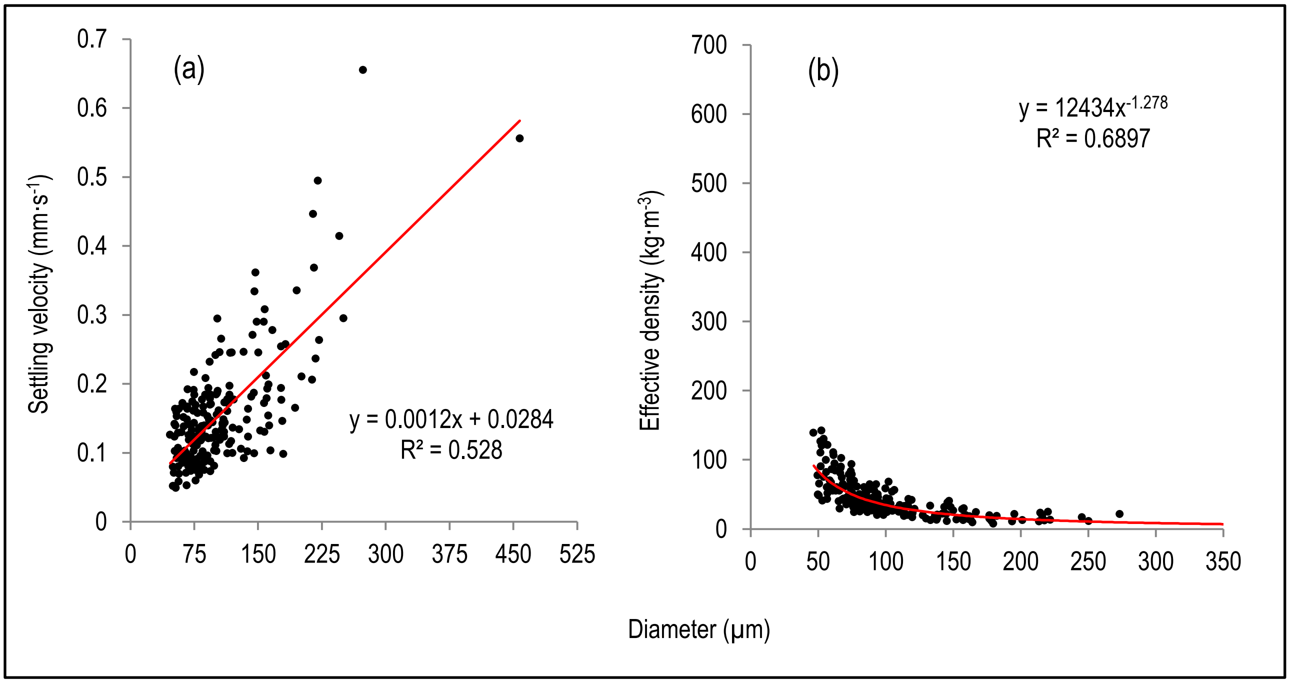

Figure 21: Size versus settling and effective density relationships, WTE 12

Settling velocity ($mm \cdot s^{-1}$) and effective particle density ($kg \cdot m^{-3}$) results for dispersed conditions, from wave tank experiment 12. Effective particle density describes the density of particles less that of seawater (1020 $g \cdot cm^{-3}$). Data are plotted as settling velocity or effective density versus particle diameter (µm) and are fitted to (a) linear and (b) power law models. Note the change in X-axis values on (a) to accommodate the occurrence of large (>350 µm) particles.

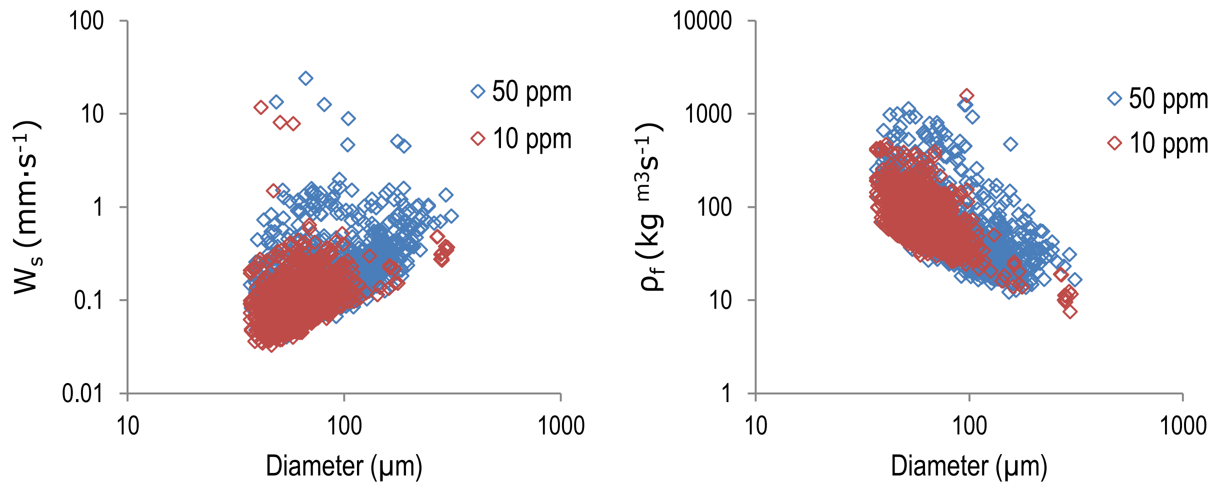

Figure 22: Size versus settling lab results

Settling velocity (w_s) ($mm \cdot s^{-1}$) and effective particle density (ρ_f) ($kg \cdot m^{-3} \cdot s^{-1}$) results from laboratory size versus settling experiments, plotted as the log of w_s or ρ_f versus the log of particle diameter (µm).

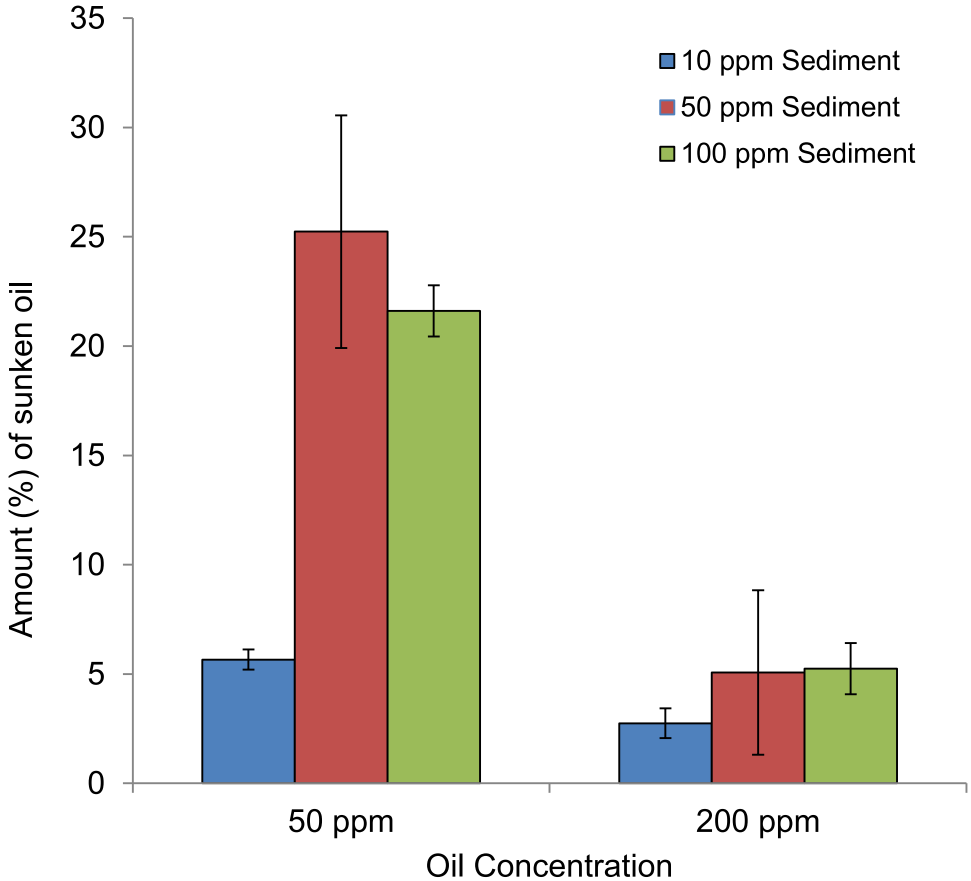

Figure 23: Amount of settled oil

Percentage of the total amount of oil added that was to the flask that sunk to the bottom during the settling experiment. Two oil concentrations (50, 200 ppm) and three sediment concentrations (10, 50, 100 ppm) were tested. At most, ~25% of the initial amount of oil sunk to the bottom.

Table 4: Size versus settling analysis

Results of size versus settling analysis for 7 wave tank experiments. Mean per-experiment values of particle size (µm), settling velocity ($mm \cdot s^{-1}$) and effective particle density (E. density) ($kg \cdot m^{-3} \cdot s^{-1}$) are shown, grouped by the presence of dispersant. Mean values for dispersed and non-dispersed groupings are also shown.

Dispersed

Experiment	Size (µm)	Settling velocity ($mm \cdot s^{-1}$)	Density ($kg \cdot m^{-3} s^{-1}$)
WTE-5	73.86	0.2067	142.69
WTE-9	91.70	0.1548	89.33
WTE-10	82.95	0.1417	98.47
Means:	82.83	0.17	110.16

Non-dispersed

Experiment	Size (µm)	Settling velocity ($mm \cdot s^{-1}$)	Density ($kg \cdot m^{-3} s^{-1}$)
WTE-4	70.03	0.2463	225.59
WTE-7	79.75	0.1281	113.82
WTE-8	88.80	0.1121	52.63
WTE-12	105.34	0.1556	50.67
Means:	85.98	0.16	110.68

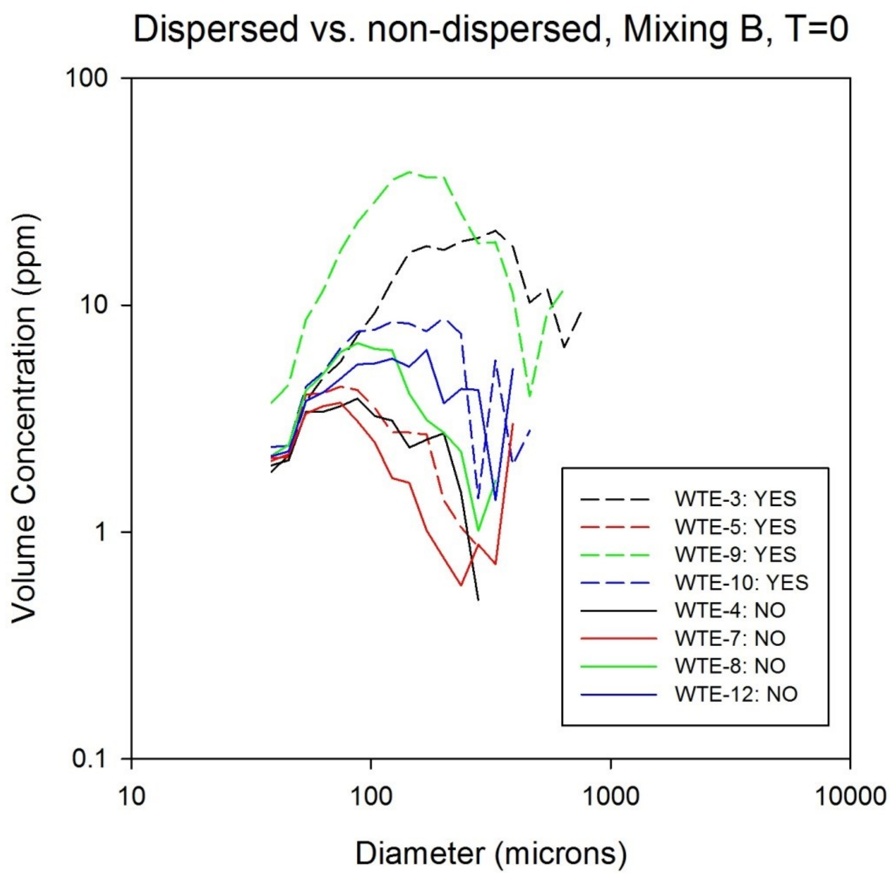

Figure 24: Particle size distributions, Mixing B (T=0)

Particle size distributions from the MVFC, immediately after oil (and dispersant, where applicable) were added (Mixing B, T = 0). Dispersed conditions are shown with solid lines, while non-dispersed conditions are shown with dashed lines. The presence and absence of dispersant is also indicated with 'yes' and 'no' in the legend.

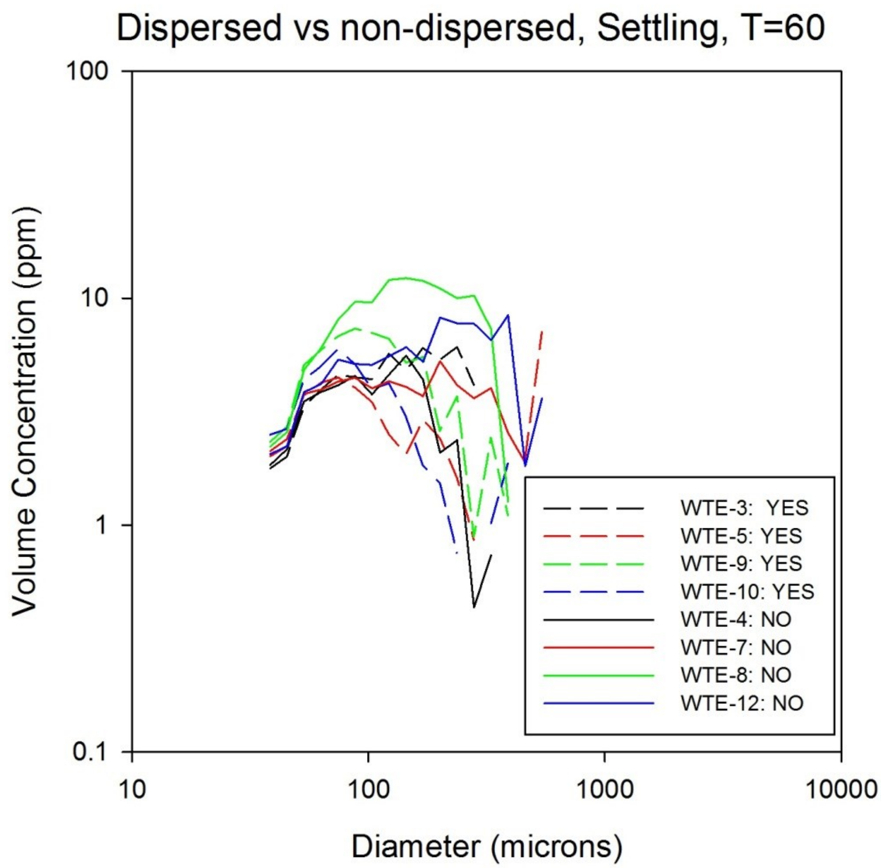

Figure 25: Particle size distributions, Settling (T=60)

Particle size distributions from the MVFC, from late in the settling phase (Settling, T = 60 min). Dispersed conditions are shown with solid lines, while non-dispersed conditions are shown with dashed lines. The presence and absence of dispersant is also indicated with 'yes' and 'no' in the legend.